CERN-EP-2018-129
2022/07/21

CMS-EXO-16-055

Search for dark matter produced in association with a Higgs boson decaying to $\gamma\gamma$ or $\tau^+\tau^-$ at $\sqrt{s} = 13$ TeV

The CMS Collaboration*

Abstract

A search for dark matter particles is performed by looking for events with large transverse momentum imbalance and a recoiling Higgs boson decaying to either a pair of photons or a pair of τ leptons. The search is based on proton-proton collision data at a center-of-mass energy of 13 TeV collected at the CERN LHC in 2016 and corresponding to an integrated luminosity of 35.9 fb^{-1} . No significant excess over the expected standard model background is observed. Upper limits at 95% confidence level are presented for the product of the production cross section and branching fraction in the context of two benchmark simplified models. For the Z' -two-Higgs-doublet model (where Z' is a new massive boson mediator) with an intermediate heavy pseudoscalar particle of mass $m_A = 300 \text{ GeV}$ and $m_{\text{DM}} = 100 \text{ GeV}$, Z' masses up to 1265 GeV are excluded. For a baryonic Z' model, with $m_{\text{DM}} = 1 \text{ GeV}$, Z' masses up to 615 GeV are excluded. Results are also presented for the spin-independent cross section for the dark matter-nucleon interaction as a function of the mass of the dark matter particle. This is the first search for dark matter particles produced in association with a Higgs boson decaying to two τ leptons.

Submitted to the Journal of High Energy Physics

1 Introduction

Astrophysical evidence strongly suggests the existence of dark matter (DM) in the universe [1]. Whether the DM has a particle origin remains a mystery [2]. There are a number of well-motivated theories beyond the standard model (SM) of particle physics that predict the existence of a particle, χ , that could serve as a DM candidate. To date, only gravitational interactions between DM and SM particles have been observed. However, the discovery of a Higgs boson by both the ATLAS and CMS Collaborations at the CERN LHC in 2012 [3–5] provides a new way to probe DM-SM particle interactions.

Collider experiment searches have typically looked for DM recoiling against an associated SM particle. Since any produced DM is unlikely to interact with the detector material, it creates an imbalance in the recorded momentum yielding a large amount of missing transverse momentum, p_T^{miss} . This paper presents a search for DM recoiling against an SM-like Higgs boson (h) using the $h + p_T^{\text{miss}}$ signature. This SM-like Higgs boson can be produced from initial- or final-state radiation, or from a new interaction between DM and SM particles. However, initial-state radiation of an SM-like Higgs boson from a quark or gluon is suppressed by Yukawa or loop processes, respectively [6–8].

Previous searches for $h + p_T^{\text{miss}}$ have been performed at both the ATLAS and CMS experiments. No excesses were observed in either $h \rightarrow b\bar{b}$ or $h \rightarrow \gamma\gamma$ decay channels with 20.3 fb^{-1} of data at $\sqrt{s} = 8 \text{ TeV}$ [9, 10] or with $2.3\text{--}36.1 \text{ fb}^{-1}$ of data at $\sqrt{s} = 13 \text{ TeV}$ [11–13]. This paper examines two Higgs boson decay channels: $h \rightarrow \gamma\gamma$ and $h \rightarrow \tau^+\tau^-$. This is the first search for DM produced in association with $h \rightarrow \tau^+\tau^-$ and the first to combine results from a combination of the $\gamma\gamma$ and $\tau^+\tau^-$ decay channels.

Two simplified models for DM+ h production are used as benchmarks for this search, both of which were recommended by the ATLAS-CMS Dark Matter Forum [14]. The leading order (LO) Feynman diagrams for these models are shown in Fig. 1. The first benchmark model (Fig. 1 left) is a Z' -two-Higgs-doublet model (Z' -2HDM) [7]. In this scenario, the SM is extended by a $U(1)_{Z'}$ group, with a new massive Z' boson mediator, while a Type-2 2HDM framework [15, 16] is used to formulate the extended Higgs sector. At LO, the Z' boson is produced resonantly and decays into an SM-like Higgs boson and an intermediate heavy pseudoscalar particle (A). The A then decays into a pair of Dirac fermionic DM particles. This analysis does not consider the contribution of the decay $Z' \rightarrow Zh$ which can have a $h + p_T^{\text{miss}}$ signature if $Z \rightarrow \nu\nu$. The second diagram (Fig. 1 right) describes a baryonic Z' model [8]. In this scenario, a new massive vector mediator Z' emits a Higgs boson and then decays to a pair of Dirac fermionic DM particles. Here, the baryonic gauge boson Z' arises from a new $U(1)_B$ baryon number symmetry. A baryonic Higgs boson (h_B) is introduced to spontaneously break the new symmetry and generates the Z' boson mass via a coupling that is dependent on the h_B vacuum expectation value. The Z' couplings to quarks and DM are proportional to the $U(1)_B$ gauge couplings. There is a mixing between h_B and the SM Higgs boson, allowing the Z' to radiate an SM-like Higgs boson. The stable baryonic states in this model are the candidate DM particles.

In the Z' -2HDM, there are several parameters that affect the predicted cross section. However, when the A is on-shell, only the Z' and A masses affect the kinematic distributions of the final state particles studied in this analysis. This paper considers a Z' resonance with mass between 450 and 2000 GeV and an A pseudoscalar with mass between 300 and 700 GeV. Masses of A below 300 GeV are excluded by constraints on flavor-changing neutral currents from $b \rightarrow s\gamma$ measurements [16] and are not considered in this analysis. The ratio of the vacuum expectation values of the Higgs doublets ($\tan\beta$) in this model is fixed to 1. As given in Ref. [12], the DM particle mass is fixed to 100 GeV, the DM- A coupling strength g_{DM} is fixed to 1, and the Z'

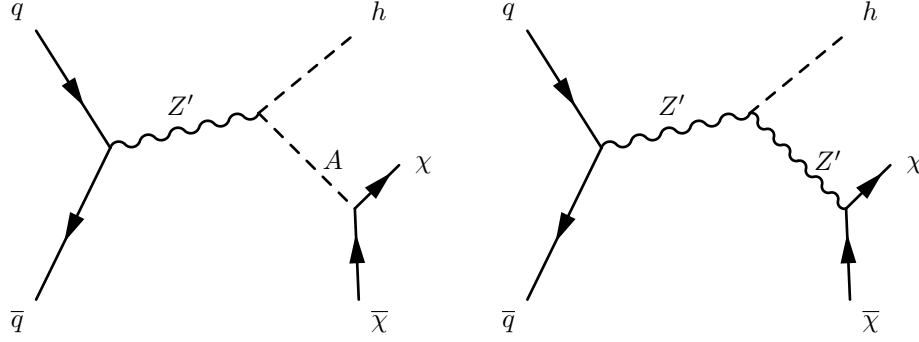


Figure 1: Leading order Feynman diagrams for DM associated production with a Higgs boson for two theoretical models: Z' -2HDM (left) and baryonic Z' (right).

coupling strength $g_{Z'}$ is fixed to 0.8.

For the baryonic Z' model, this paper considers a Z' resonance with a mass between 10 and 2500 GeV and DM particle masses between 1 and 900 GeV. As suggested for this model [17], the mediator-DM coupling is fixed to 1 and the mediator-quark coupling (g_q) is fixed to 0.25. The mixing angle between the baryonic Higgs boson and the SM-like Higgs boson is set to 0.3 and the coupling between the Z' boson and the SM-like Higgs boson is proportional to the mass of the Z' boson.

For both models, values of the couplings and mixing angle are chosen to maximize the predicted cross section. Results for other values can be obtained by rescaling the cross section since these parameters do not affect the kinematic distributions of the final state particles. The SM-like Higgs boson is assumed to be the already observed 125 GeV Higgs boson, since the SM-like Higgs boson has similar properties to the SM Higgs boson. Therefore, in this paper the observed 125 GeV Higgs boson is denoted by h .

Although the SM Higgs boson branching fractions to $\gamma\gamma$ and $\tau^+\tau^-$ are smaller than the branching fraction to $b\bar{b}$, the analysis presented here exploits these two decay channels because they have unique advantages compared with the $h \rightarrow b\bar{b}$ channel. The $h \rightarrow \gamma\gamma$ channel benefits from higher precision in reconstructed invariant mass and the $h \rightarrow \tau^+\tau^-$ channel benefits from smaller SM background. Additionally, the $h \rightarrow \gamma\gamma$ and $h \rightarrow \tau^+\tau^-$ channels are not dependent on p_T^{miss} trigger thresholds, as such searches in these channels are complementary to those in the $h \rightarrow b\bar{b}$ channel since they can probe DM scenarios with lower p_T^{miss} . The search in the $h \rightarrow \gamma\gamma$ channel uses a fit in the diphoton invariant mass spectrum to extract the signal yield. In addition to a high- p_T^{miss} category, a low- p_T^{miss} category is also considered to extend the phase space of the search. In the $h \rightarrow \tau^+\tau^-$ channel, the three decay channels of the τ lepton with the highest branching fractions are analyzed. After requiring an amount of p_T^{miss} in order to sufficiently suppress the quantum chromodynamic (QCD) multijet background, the signal is extracted by performing a simultaneous fit to the transverse mass of the p_T^{miss} and the two τ lepton candidates in the signal region (SR) and control regions (CRs).

The paper is organized as follows. Section 2 gives a brief description of the CMS detector and the event reconstruction. Section 3 details the data set and the simulated samples used in the analysis. Then Sections 4 and 5 present the event selection and analysis strategy for each decay channel, respectively. The systematic uncertainties affecting the analysis are presented in Section 6. Section 7 details the results of the analysis and their interpretations. A summary is given in Section 8.

2 The CMS detector and event reconstruction

The central feature of the CMS detector is a superconducting solenoid, of 6 m internal diameter, providing an axial magnetic field of 3.8 T along the beam direction. Within the solenoid volume are a silicon pixel and strip tracker, a lead-tungstate crystal electromagnetic calorimeter (ECAL), and a brass and scintillator hadron calorimeter (HCAL). Extensive forward calorimetry complements the coverage provided by the barrel and endcap detectors. Charged particle trajectories are measured by the silicon pixel and strip tracker system, covering $0 \leq \phi \leq 2\pi$ in azimuth and $|\eta| < 2.50$, where the pseudorapidity is $\eta = -\ln(\tan \theta/2)$, and θ is the polar angle with respect to the counterclockwise beam direction. Muons are measured in gas-ionization detectors embedded in the steel flux-return yoke. A more detailed description of the CMS detector can be found in Ref. [18].

Events of interest are selected using a two-tiered trigger system [19]. The first level, composed of custom hardware processors, uses information from the calorimeters and muon detectors to select events at a rate of around 100 kHz within a time interval of less than $4 \mu\text{s}$. The second level, known as the high-level trigger, consists of a farm of processors running a version of the full event reconstruction software optimized for fast processing, and reduces the event rate to around 1 kHz before data storage.

Using information from all CMS subdetectors, a global event reconstruction is performed using the particle-flow (PF) algorithm [20]. The PF algorithm optimally combines all of the detector information and generates a list of stable particles (PF candidates), namely photons, electrons, muons, and charged and neutral hadrons. The reconstructed vertex with the largest value of summed physics-object p_T^2 is taken to be the primary pp interaction vertex (PV). The physics objects are the jets, clustered using the jet finding algorithm [21, 22] with the tracks assigned to the vertex as inputs, and the negative vector sum of the p_T of those jets. The PV is used as the reference vertex for all objects reconstructed with the PF algorithm.

Photons are reconstructed from their energy deposits in the ECAL, which can involve several crystals [23]. A photon that converts to an electron-positron pair in the tracker will yield a shower spread out in azimuth due to the deflection of the electron and positron in the strong magnetic field. In order to achieve the best photon energy resolution, corrections are applied to overcome energy losses including those from photon conversions [23]. Additional corrections, calculated from the mass distribution of $Z \rightarrow e^+e^-$ events, are applied to the measured energy scale of the photons in data ($\leq 1\%$) and to the energy resolution in simulation ($\leq 2\%$).

Electron reconstruction requires the matching of the cluster of energy deposits in the ECAL with a track in the silicon tracker. Electron identification is based on the ECAL shower shape, matching between the track and ECAL cluster, and consistency with the PV. Muons are reconstructed by combining two complementary algorithms [24]: one that matches tracks in the silicon tracker with signals in the muon system, and another in which a global track fit seeded by the muon track segment is performed.

Jets are reconstructed from PF candidates using the anti- k_T clustering algorithm [21] as implemented in FASTJET [22] with a distance parameter of 0.4. Jet energy corrections are derived from simulation to bring the average measured response of jets to that of particle-level jets. Hadronically decaying τ leptons are reconstructed from jets using the hadrons-plus-strips (HPS) algorithm [25]. The HPS algorithm uses combinations of reconstructed charged hadrons and energy deposits in the ECAL to reconstruct the τ lepton's three most common hadronic decay modes: 1-prong, 1-prong + $\pi^0(s)$, and 3-prong. In the $h \rightarrow \tau^+\tau^-$ channel, events with jets originating from b quark decays are excluded in order to reduce the background from $t\bar{t}$

events. The combined secondary vertex algorithm [26] is used to identify jets originating from b quarks by their characteristic displaced vertices.

The missing transverse momentum vector (\vec{p}_T^{miss}), with magnitude p_T^{miss} , is the negative vector sum of the p_T of all PF candidates in an event. Jet energy corrections are propagated to the \vec{p}_T^{miss} for a more accurate measurement [27]. Events may have anomalously large p_T^{miss} from sources such as detector noise, cosmic ray muons, and beam halo particles, which are not well modeled in simulation. Event filters [28] are applied to remove such events.

3 Observed and simulated data samples

The analysis is performed with pp collision data at $\sqrt{s} = 13$ TeV collected with the CMS detector in 2016. The data correspond to an integrated luminosity of 35.9 fb^{-1} .

The analysis strategy and event selection were optimized using Monte Carlo (MC) simulated samples of associated DM+h production via the two benchmark models discussed in Section 1. The MADGRAPH5_aMC@NLO v2.3.0 [29] generator is used to generate both the Z' -2HDM and baryonic Z' signals at LO. The decay of the SM-like Higgs boson is simulated by PYTHIA 8.205 [30].

A small but irreducible background for both decay channels in this analysis comes from events in which the SM Higgs boson is produced in association with a Z boson that decays to two neutrinos. Other SM Higgs boson production mechanisms are associated with resonant but reducible backgrounds. These include gluon-gluon fusion (ggh), vector boson fusion (VBF), and production in association with a pair of top quarks ($t\bar{t}$). The production in association with a vector boson (Vh) and other SM Higgs boson backgrounds are all generated using MADGRAPH5_aMC@NLO v2.2.2 at next-to-leading order (NLO) in perturbative QCD.

The dominant nonresonant backgrounds for the $h \rightarrow \gamma\gamma$ channel are events with mismeasured p_T^{miss} and two photons that happen to have an invariant mass close to the mass of the SM Higgs boson. The largest contributions to this are nonresonant $\gamma\gamma$, $\gamma + \text{jet}$, and QCD multijet production. The simulated $\gamma\gamma$ sample is generated at LO with SHERPA v2.2.2 [31] while the $\gamma + \text{jet}$ and QCD multijet samples are modeled at LO with PYTHIA. Additional backgrounds originate from electroweak (EW) processes such as single top, $t\bar{t}$, W, or Z boson production in association with one or two photons, and Drell-Yan (DY) production where the Z boson decays to pairs of electrons or muons. The DY and all other EW backgrounds considered in the analysis are generated at NLO with MADGRAPH5_aMC@NLO. These nonresonant background samples are used for optimizing the analysis selection, however, they are not used for the ultimate background estimation.

The largest backgrounds for the $h \rightarrow \tau^+\tau^-$ channel are W + jets, $t\bar{t}$, and multiboson processes. The MADGRAPH5_aMC@NLO v2.3.0 generator is used for W + jets processes, which are generated at LO in perturbative QCD with the MLM jet matching and merging scheme [32]. A p_T -dependent correction factor is applied to the W + jets sample to account for next-to-next-to-leading order QCD and NLO EW effects [33–36]. The $t\bar{t}$ process is generated at NLO with the POWHEG 2.0 [37–40] generator. Single top quark production is modeled at NLO with the POWHEG 1.0 [41] generator. The FxFx [42] merging scheme is used to generate some smaller diboson backgrounds (including WZ samples) with the MADGRAPH5_aMC@NLO generator at NLO, while the dominant diboson backgrounds, WW and ZZ in two lepton final states, are generated using POWHEG 2.0. Another reducible background considered in this analysis is $Z/\gamma^* \rightarrow \ell\ell/\tau\tau$, where ℓ is e or μ . The Drell-Yan background which is corrected for differences

in the dilepton mass $m_{\ell\ell/\tau\tau}$ and dilepton transverse momentum $p_T(\ell\ell/\tau\tau)$ distributions using dimuon events in data [43].

All simulated samples mentioned above use the NNPDF 3.0 parton distribution function (PDF) sets [44, 45] with the order matching that used in the matrix element calculations. For parton showering and hadronization, as well as for τ lepton decays, the samples are interfaced with PYTHIA using the CUETP8M1 tune [46] for all samples except $t\bar{t}$, for which the M2 tune is used. The MC samples are processed through a full simulation of the CMS detector based on GEANT4 [47] and are reconstructed with the same algorithms that are used for the data. All samples include the simulation of additional inelastic pp interactions in the same or neighboring bunch crossings (pileup). Minimum-bias collision events generated with PYTHIA are added to the simulated samples to reproduce the pileup effects in the data. Additionally, the simulated events are weighted so that the pileup vertex distribution matches that of the data, with an average of 27 interactions per bunch crossing.

4 Analysis strategy in the $h \rightarrow \gamma\gamma$ channel

The search for DM+h in the $h \rightarrow \gamma\gamma$ channel is performed by selecting events with two photons and a large amount of p_T^{miss} . The set of requirements detailed in Section 4.1 is applied to select well-identified photons and to enhance the signal significance. A fit to the diphoton invariant mass distribution, described in Section 4.2, is performed to extract the background and signal yields.

4.1 Event selection

The events used in this analysis were selected by a diphoton trigger with asymmetric p_T thresholds of 30 and 18 GeV. The trigger also has loose photon identification criteria based on the cluster shower shape, isolation requirements, and a selection on the ratio of hadronic to electromagnetic energy deposits of the photon candidates.

The photons that enter the analysis are required to fall within the fiducial range of the ECAL ($|\eta| < 1.44$ or $1.57 < |\eta| < 2.50$) and to satisfy various preselection criteria that are slightly more stringent than the trigger requirements. An additional veto on the presence of a track pointing to the ECAL cluster is applied to reject electrons that could be reconstructed as photons. Scale factors, extracted from $Z \rightarrow e^+e^-$ events using the tag-and-probe method [48], are applied to the simulated samples to account for any discrepancy in identification efficiency between data and simulation.

The isolation variables that are used in the photon identification are calculated by summing the p_T of PF photons, neutral hadrons, or charged hadrons associated with the PV in a cone of radius $\Delta R = \sqrt{(\Delta\eta)^2 + (\Delta\phi)^2} = 0.3$. The isolation variables are corrected by the median transverse momentum density of the event to mitigate the effects of pileup [49]. Some of the signals considered can have Lorentz-boosted topologies. For example, high-mass mediators could result in a large boost to the Higgs boson. When a boosted Higgs boson decays to two photons, the resulting photons hit the ECAL close to each other. This effect leads to large contributions from one photon to the photon isolation sum of the other. In order to maintain high efficiency for high-mass mediator signals, the photon isolation requirement is not applied to photons that are within $\Delta R < 0.3$ of each other.

Preselected photons are required to have leading (subleading) photon p_T above 30 (20) GeV and diphoton invariant mass $m_{\gamma\gamma}$ above 95 GeV. Simulated signal and background samples

that pass the preselection were used to study the discriminating power of variables such as p_T^{miss} , the p_T of the diphoton system $p_{T\gamma\gamma}$, and the ratio $p_T/m_{\gamma\gamma}$ for each photon. A selection on p_T that scales with $m_{\gamma\gamma}$ is chosen so that it does not distort the shape of the $m_{\gamma\gamma}$ distribution. The $p_{T\gamma\gamma}$ variable is included in the selection because it has higher resolution than the event's measured p_T^{miss} and is expected to be large for signal events, since the Higgs boson is produced back-to-back with \vec{p}_T^{miss} . A high- p_T^{miss} category ($p_T^{\text{miss}} \geq 130$ GeV) is optimal for the two benchmark models presented in this paper. A low- p_T^{miss} category ($50 < p_T^{\text{miss}} < 130$ GeV), optimized using as reference the baryonic Z' signal model, is also included to probe softer signals, namely signals that may not be observed in other $h + p_T^{\text{miss}}$ searches because they rely heavily on p_T^{miss} for background rejection. The chosen requirements, found to optimize the signal sensitivity for both models in the low- and high- p_T^{miss} categories, are given in Table 1.

Table 1: Optimized kinematic requirements for the low- and high- p_T^{miss} categories.

Variable	Low- p_T^{miss} category	High- p_T^{miss} category
p_T^{miss}	>50 GeV, <130 GeV	>130 GeV
$p_{T1}/m_{\gamma\gamma}$	>0.45	>0.5
$p_{T2}/m_{\gamma\gamma}$	>0.25	>0.25
$p_{T\gamma\gamma}$	>75 GeV	>90 GeV

Further background rejection is achieved using two topological requirements. The azimuthal separation $|\Delta\phi(p_{\gamma\gamma}, \vec{p}_T^{\text{miss}})|$ between \vec{p}_T^{miss} and the Higgs boson direction reconstructed from the two photons must be greater than 2.1 to select events in which the Higgs boson and \vec{p}_T^{miss} are back-to-back. Events with highly energetic jets collinear to \vec{p}_T^{miss} are removed by the requirement that the $\min|\Delta\phi(p_{\text{jet}}, \vec{p}_T^{\text{miss}})|$ be greater than 0.5 for any jet with p_T above 50 GeV. This rejects events with a large misreconstructed p_T^{miss} arising from mismeasured jet p_T . Finally, events are vetoed if they have three or more jets each with p_T above 30 GeV, to reject multijet backgrounds while maintaining a high efficiency for the two benchmark signal models. The p_T^{miss} distribution of the selected events is shown in Fig. 2.

4.2 Background estimation and signal extraction

A narrow resonance search similar to the SM Higgs boson diphoton analysis of Ref. [50] is performed. The diphoton invariant mass between 105 and 180 GeV is fit with a model that is the sum of the signal and background shapes. The signal shape, taken from the simulated events, is allowed to change independently in each of the two p_T^{miss} categories. The background shape includes a smooth function, estimated from the data, to model the continuum background, and a resonant contribution from the SM Higgs boson. The fit is performed with an unbinned maximum-likelihood technique in both the low- and high- p_T^{miss} categories discussed above.

The resonant background, arising from the SM Higgs boson decays to two photons, appears as a peak under the expected signal peak. This contribution from all SM Higgs boson production modes is estimated with the simulated events by including a mass distribution template, scaled to the NLO cross section, as a resonant component in the final fitting probability density function (pdf).

The nonresonant background contribution, mostly due to $\gamma\gamma$ and to various EW processes, is estimated using data. The nonresonant diphoton $m_{\gamma\gamma}$ distribution in the data is fit, in each p_T^{miss} category, with an analytic function. Because the exact functional form of the background is unknown, the parametric model must be flexible enough to describe a variety of potential underlying functions. Using an incorrect background model can lead to biases in the measured signal yield that can artificially modify the sensitivity of the analysis. Three functions are considered as possible models for the nonresonant background; they are analytical forms that are

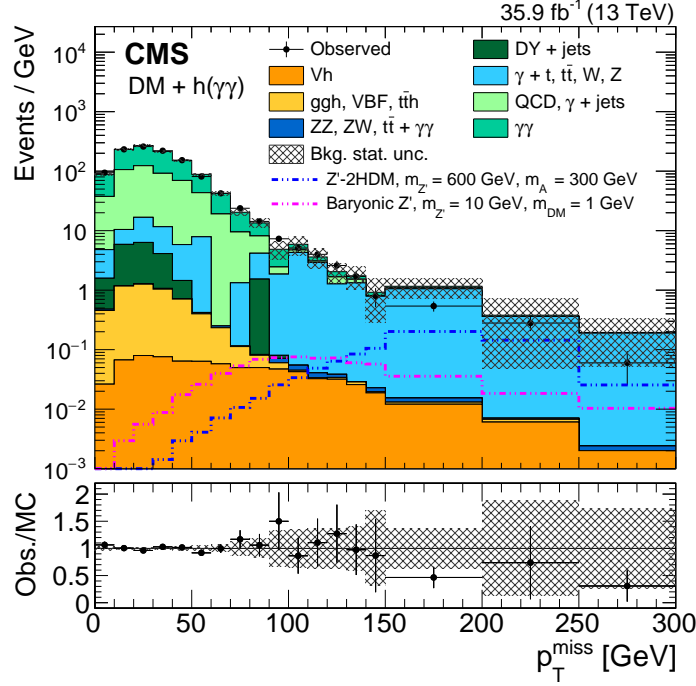


Figure 2: Distribution of p_T^{miss} for events passing the requirements given in Table 1. Events with p_T^{miss} below 50 GeV are not used in the analysis. The cross sections of the signals are set to 1 pb. The total simulated background is normalized to the integral of the data. The statistical uncertainty in the total background is shown by the hatched bands. The data-to-simulation ratio is shown in the lower panel.

frequently used in dijet [51] and diphoton [52] resonance searches. The best functional form found to fit the nonresonant diphoton $m_{\gamma\gamma}$ distribution, in both p_T^{miss} categories, is a power law function $f(x) = ax^{-b}$ where a and b are free parameters constrained to be positive.

A detailed bias study has been performed in order to choose this function. The $m_{\gamma\gamma}$ shape of the simulated nonresonant events is used as a template to generate 1000 pseudo-experiments for each p_T^{miss} category. For each pseudo-experiment, the number of events generated is equal to the number of events observed in data in that category. The resulting $m_{\gamma\gamma}$ distribution is fit with each analytic function considered. The exercise is also repeated injecting a potential signal contribution. The pulls of each pseudo-experiment, defined as the difference in the number of simulated events and those predicted by the fit function divided by the statistical uncertainties of the fit, are calculated. If the bias (the median of the pulls) is five times smaller than the statistical uncertainty in the number of fitted signal events, any potential bias from the choice of background model is considered negligible. Since this criterion is satisfied for the power law function, any systematic uncertainty in the bias from the background fit function is neglected in this analysis.

The final background-only fit for both p_T^{miss} categories is shown in Fig. 3. Both the resonant and nonresonant background pdf contributions are shown. The slight excess of events observed in data around 125 GeV in the low- p_T^{miss} category is compatible with the SM Higgs boson expectation within 2.0 standard deviations.

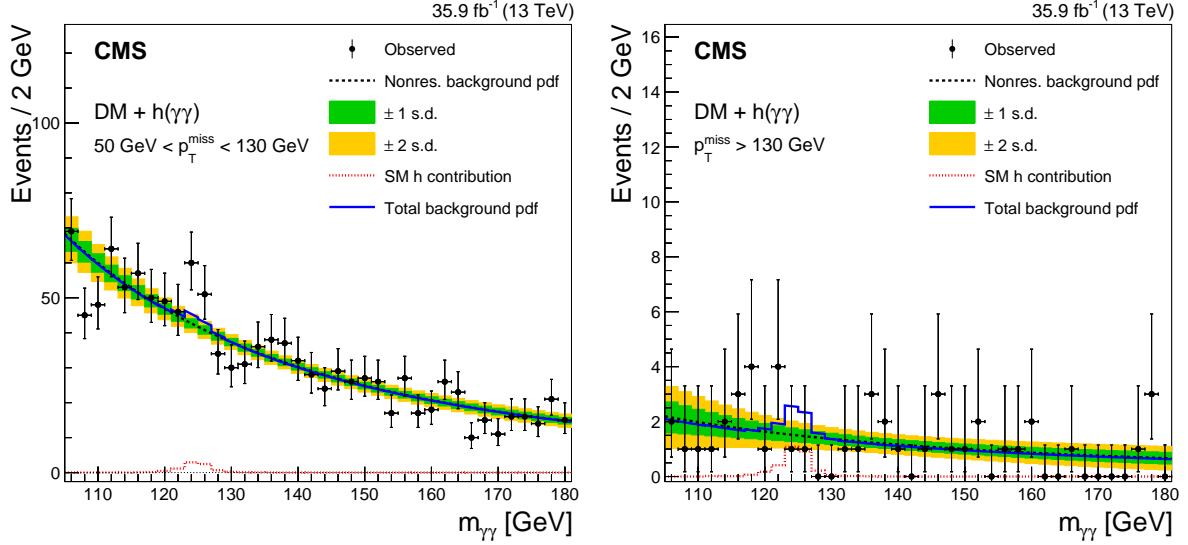


Figure 3: The background-only fit to data is performed, for low- p_T^{miss} (left) and high- p_T^{miss} (right) categories, with the sum of a power law (dashed black) fit function to describe the non-resonant contribution, and a resonant shape (dashed red), taken from simulation, to take into account the SM $h \rightarrow \gamma\gamma$ contribution. The SM h contribution is fixed to the theoretical prediction in the statistical analysis. The sum of the nonresonant and resonant shapes (solid blue) is used to estimate the total background in this analysis.

5 Analysis strategy in the $h \rightarrow \tau^+\tau^-$ channel

5.1 Event selection

The three final states of τ lepton pairs with the highest $\tau\tau$ branching fractions ($e\tau_h$, $\mu\tau_h$, and $\tau_h\tau_h$) are considered in this analysis. In the $e\tau_h$ and $\mu\tau_h$ channels, one of the τ leptons decays leptonically to an electron or a muon and two neutrinos, while the other τ lepton decays hadronically (τ_h). In the third channel, $\tau_h\tau_h$, both τ leptons decay hadronically. The $e\mu$, ee , and $\mu\mu$ final states are not included because of the low branching fraction of the $\tau\tau$ pair to purely leptonic final states. The ee and $\mu\mu$ final states are not considered, since they are overwhelmed by DY background.

Triggers based on the presence of a single electron (muon) are used to select events in the $e\tau_h$ ($\mu\tau_h$) channel. In the $\tau_h\tau_h$ channel, the triggers require the presence of two isolated τ_h objects. Each τ_h candidate reconstructed offline is required to match a τ_h candidate at the trigger level, with a ΔR separation less than 0.5.

The electrons and muons in the $e\tau_h$ and $\mu\tau_h$ channels are required to have p_T greater than 26 GeV, exceeding the trigger thresholds for the single-electron and single-muon triggers. Electrons (muons) with $|\eta| < 2.1$ (2.4) are used. An $e\tau_h$ ($\mu\tau_h$) event is required to have an electron (muon) passing a multivariate MVA identification discriminator (straightforward selection identification criteria) and an isolation requirement of $I_{\text{rel}}^e < 0.10$ ($I_{\text{rel}}^\mu < 0.15$), where I_{rel}^ℓ is defined as in Eq. (1), with an isolation cone of size $\Delta R = 0.3$ (0.4) surrounding the electron (muon):

$$I_{\text{rel}}^\ell = \left(\sum p_T^{\text{charged}} + \max[0, \sum p_T^{\text{neutral}} + \sum p_T^\gamma - 0.5 \times \sum p_T^{\text{PU}}] \right) / p_T^\ell. \quad (1)$$

Here $\sum p_T^{\text{charged}}$, $\sum p_T^{\text{neutral}}$, and $\sum p_T^\gamma$ are the scalar sums of transverse momentum from charged hadrons associated with the primary vertex, neutral hadrons, and photons, respectively. The

term $\sum p_T^{\text{PU}}$ is the sum of transverse momentum of charged hadrons not associated with the primary vertex and p_T^ℓ is the p_T of the electron or muon.

Hadronically decaying τ leptons in all channels are required to satisfy a loose ($\tau_h \tau_h$ channel) or a tight ($e\tau_h$ and $\mu\tau_h$ channels) working point of an MVA isolation measure. The loose (tight) working point corresponds to a 65 (50)% efficiency with a 0.8 (0.2)% misidentification probability. The τ leptons are required to be identified as decaying via one of the three modes recognized with the HPS algorithm, and also pass discriminators that reduce the rate of electrons and muons misreconstructed as τ_h candidates [53]. For the $e\tau_h$ and $\mu\tau_h$ channels, the τ_h candidates are required to have $p_T > 20$ GeV and $|\eta| < 2.3$. In the $\tau_h \tau_h$ channel, the leading (subleading) τ lepton p_T is required to be greater than 55 (40) GeV, both τ_h momenta exceeding the double-hadronic τ lepton trigger thresholds of 35 GeV. The selection criteria are summarized in Table 2 for all three final states.

Table 2: Selection requirements for the three $\tau\tau$ decay channels. The p_T thresholds for the triggers are given in the second column in parentheses.

Final state	Trigger type	Lepton selection		
		p_T [GeV]	η	Isolation
$e\tau_h$	e(25 GeV)	$p_T^e > 26$	$ \eta^e < 2.1$	$I_{\text{rel}}^e < 0.1$
		$p_T^{\tau_h} > 20$	$ \eta^{\tau_h} < 2.3$	Tight MVA τ_h
$\mu\tau_h$	μ (24 GeV)	$p_T^\mu > 26$	$ \eta^\mu < 2.4$	$I_{\text{rel}}^\mu < 0.15$
		$p_T^{\tau_h} > 20$	$ \eta^{\tau_h} < 2.3$	Tight MVA τ_h
$\tau_h \tau_h$	τ_h (35 GeV) & τ_h (35 GeV)	$p_T^{\tau_h} > 55 \text{ \& } 40$	$ \eta^{\tau_h} < 2.1$	Loose MVA τ_h

The p_T^{miss} is further required to be greater than 105 GeV and the visible p_T of the $\tau\tau$ system is required to be greater than 65 GeV. These stringent criteria reduce the need for tighter isolation in the $\tau_h \tau_h$ channel. Additionally, the mass reconstructed from the visible p_T of the $\tau\tau$ system is required to be less than 125 GeV, to ensure that the $\tau\tau$ system is compatible with an SM Higgs boson. In order to minimize diboson and W + jets contributions, the two τ lepton candidates must pass a loose collinearity criterion of $\Delta R_{\tau\tau} < 2.0$.

Two types of event veto are employed for background reduction. Events with jets tagged as originating from hadronization of b quarks are vetoed, to reduce $t\bar{t}$ and single top processes. The working point used in the b tagging algorithm corresponds to about a 66% efficiency for a 1% misidentification probability. In addition, events with additional muons or electrons beyond those from the τ lepton candidates are discarded, to reduce the contribution of multilepton backgrounds.

5.2 Signal extraction and background estimation

The signal is extracted from a maximum-likelihood fit to the total transverse mass (M_T^{tot}) distributions in the different channels for the SR, and for the W + jets and QCD multijet background CRs. The M_T^{tot} is defined as:

$$M_T^{\text{tot}} = \sqrt{(p_T^{\tau_1} + p_T^{\tau_2} + p_T^{\text{miss}})^2 - (p_x^{\tau_1} + p_x^{\tau_2} + p_x^{\text{miss}})^2 - (p_y^{\tau_1} + p_y^{\tau_2} + p_y^{\text{miss}})^2}, \quad (2)$$

where p_x^{miss} and p_y^{miss} are the magnitudes of the x and y components of \vec{p}_T^{miss} , respectively.

The W + jets and the QCD multijet background are estimated directly from the data. The procedure to estimate these processes relies on CRs, which are included in the maximum-likelihood fit, to extract the results. The other backgrounds, $t\bar{t}$, Z + jets, SM Higgs boson, single top quark, and diboson production processes, are extracted from simulation.

The shape of the M_T^{tot} distribution of the $W + \text{jets}$ background is estimated from simulation by requiring the same selection as for the SR, but the isolation of the τ lepton candidates is relaxed to increase the statistical precision of the distribution. To constrain the normalization of the $W + \text{jets}$ background, a CR enriched in $W + \text{jets}$ events is constructed by inverting the isolation criteria on the τ_h candidates while keeping a loose isolation. The CR obtained by inverting the isolation criterion is included in the maximum-likelihood fit to constrain the normalization of the $W + \text{jets}$ background in the SR.

To estimate the QCD multijet background, a CR in data is obtained by requiring the τ lepton candidates to have the same sign. No significant amount of signal and of background with opposite-sign τ_h is expected in this CR because the τ_h charge misidentification is of order 1% and the charge misidentification for electrons and muons is even smaller. All simulated backgrounds are subtracted from observed events in the CR, and the remaining contribution is classified as QCD multijet background. The contribution of QCD multijet events with opposite-sign τ lepton candidates in the SR is obtained by multiplying the QCD multijet background, obtained in the same-sign CR, by a scale factor. The scale factor, approximately unity with an uncertainty of 20%, is determined from events with τ_h candidates failing the isolation requirement and with low p_T^{miss} , which do not overlap with events selected in the SR. To increase the statistical precision of the QCD multijet distribution, the isolation of the τ lepton candidates is relaxed for the $\ell\tau_h$ channels, while conserving the normalization obtained as detailed above. The same-sign τ lepton candidate CR constrains the QCD multijet background normalization in the SR and the other CRs in the maximum-likelihood fit.

The normalizations of the $W + \text{jets}$ and QCD multijet background are strongly correlated since both processes contribute to both CRs. The simultaneous fit of the SR and CRs takes into account this correlation. The SR distributions included in the simultaneous maximum-likelihood fit are shown in Fig. 4. For the signal extraction, $W + \text{jets}$ and QCD multijet background CRs are considered separately, whereas in Fig. 4, the two backgrounds are presented merged together.

6 Systematic uncertainties

In both analysis channels, an uncertainty of 2.5% is used for the normalization of simulated samples to reflect the uncertainty in the integrated luminosity measurement in 2016 [54]. Common to both analysis channels are systematic uncertainties related to the theoretical production cross section of the Higgs boson. The PDF, and renormalization and factorization scale uncertainties are addressed using the recommendations of PDF4LHC [55] and LHC Higgs Cross Section [56] working groups, respectively. The value of these uncertainties range from 0.3 to 9.0%. The systematic uncertainties associated with each of the analysis channels are detailed below. Uncertainties affecting normalizations are represented by log-normal pdfs in the statistical analysis.

6.1 The $h \rightarrow \gamma\gamma$ channel

In the $h \rightarrow \gamma\gamma$ channel, there are several sources of experimental and theoretical uncertainties that affect the signal and the SM $h \rightarrow \gamma\gamma$ yields. However, the largest source of uncertainty is statistical. As mentioned in Section 4.2, no systematic uncertainties are applied to the non-resonant background, which is extracted from a fit to data, since the bias of the fit is negligible compared to the statistical uncertainty of the data set. The systematic uncertainties for the $h \rightarrow \gamma\gamma$ channel are summarized in Table 3. In addition to the theoretical uncertainties mentioned above, a 20% cross section uncertainty is included for the ggh sample, based on the

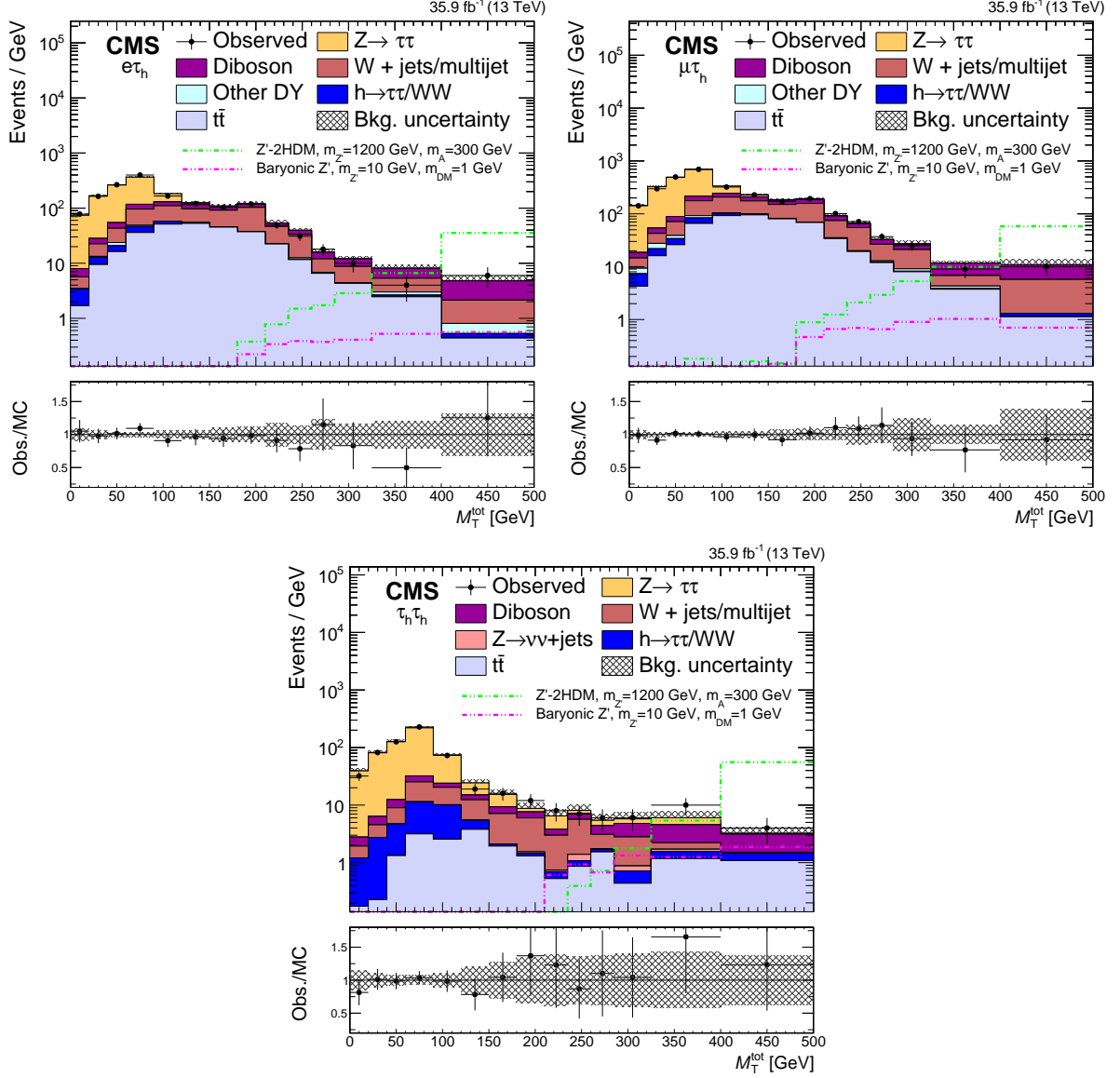


Figure 4: Distributions of the total transverse mass M_T^{tot} in the SR for the $e\tau_h$ (upper left), $\mu\tau_h$ (upper right), and $\tau_h\tau_h$ (lower) final states are shown after the simultaneous maximum-likelihood fit. Representative signal distributions are shown with cross sections normalized to 1 pb. The data points are shown with their statistical uncertainties, and the point in the final bin includes overflow. The statistical uncertainty of the observed distribution is represented by the error bars on the data points. The overflow of each distribution is included in the final 400–500 GeV bin. Single top processes are included in the “Diboson” contribution. The “Other DY” contribution includes background from $Z \rightarrow \ell\ell$. The systematic uncertainty related to the background prediction is indicated by the shaded band.

CMS differential measurements of $h \rightarrow \gamma\gamma$, for diphoton p_T above 70 GeV [57]. The branching fraction uncertainty [56] of 1.73% is also included.

In addition to the integrated luminosity uncertainty, several other experimental sources of systematic uncertainty are included in this analysis. The trigger efficiency uncertainty (approximately 1%) is extracted from $Z \rightarrow e^+e^-$ events using a tag-and-probe technique [48]. The photon identification uncertainty of 2% arises from the observed difference in efficiencies between data and simulation. A 0.5% energy scale uncertainty is assigned to take into account the knowledge of the photon energy scale at the Z boson mass peak and its extrapolation to the Higgs boson mass. Additionally, several p_T^{miss} -related uncertainties are applied. The systematic uncertainty from mismeasured p_T^{miss} is evaluated by comparing the tail of the p_T^{miss} distributions in data and simulation in a $\gamma + \text{jet}$ enriched CR. The efficiencies with which data and simulated events pass the p_T^{miss} selection are compared. The difference in efficiency is 50% and is included as a systematic uncertainty associated with mismeasured p_T^{miss} . However, the contribution of simulated backgrounds with mismeasured p_T^{miss} is quite small since only the ggh and VBF SM $h \rightarrow \gamma\gamma$ production modes contribute. Finally, a systematic uncertainty, which is less than 4%, is applied to take into account the difference in efficiency between data and simulation when applying the topological $\Delta\phi$ requirements in the low- p_T^{miss} region. This uncertainty is evaluated using $Z \rightarrow e^+e^-$ events, and only affects the ggh and VBF simulated samples.

Table 3: Systematic uncertainties affecting the signal and resonant backgrounds in the $h \rightarrow \gamma\gamma$ channel.

	Signal [%]	SM h [%]
Theoretical sources		
PDF	—	2–4
Renorm. and fact. scale	—	0.3–9
Cross section (ggh)	—	20
Higgs boson branching fraction	1.73	
Experimental sources		
Integrated luminosity	2.5	
Trigger efficiency	1.0	
Photon identification efficiency	2.0	
Photon energy scale	0.5	
p_T^{miss} mismeasurement (ggh and VBF)	—	50
$\Delta\phi$ selection efficiency (ggh and VBF)	—	1–4

6.2 The $h \rightarrow \tau^+\tau^-$ channel

The systematic uncertainties in the $h \rightarrow \tau^+\tau^-$ channel are related to the normalization of signal and background processes and, in several instances, the shapes of the signal and background distributions. As mentioned earlier, the simultaneous maximum-likelihood fit is performed in the SR and CRs, where the shape and normalization uncertainties are represented by nuisance parameters in the likelihood. Uncertainties affecting the distribution of M_T^{tot} (shape uncertainties) are represented by Gaussian pdfs, whereas log-normal pdfs are used for normalization, as stated above. The largest overall uncertainty is statistical. Table 4 summarizes the different sources of systematic uncertainty in this channel.

An uncertainty of 2% is assigned to simulated events containing an electron or muon candidate. In simulated events with a τ_h candidate, an additional uncertainty of 5% per τ_h is applied. These uncertainties account for the observed differences in the performance of electron, muon, and τ_h identification, isolation, and trigger algorithms, between data and simulation.

Table 4: Systematic uncertainties affecting signal and background in the $h \rightarrow \tau^+ \tau^-$ channel.

Source	Affected processes	Change in acceptance or shape		
		$e\tau_h$	$\mu\tau_h$	$\tau_h\tau_h$
τ_h identification (correlated)	simulation	4.5%	4.5%	—
τ_h identification (uncorrelated)	simulation	2%	2%	9%
High p_T τ_h	simulation		Shape, up to 8%	
e identification & trigger	simulation	2%	—	—
μ identification & trigger	simulation	—	2%	—
τ_h trigger	simulation	—	—	Shape only
e misidentified as τ_h	$Z \rightarrow ee$	12%	—	—
μ misidentified as τ_h	$Z \rightarrow \mu\mu$	—	25%	—
Jet misidentified as τ_h	$Z + \text{jets}$		Shape only	
τ_h energy scale (per decay mode)	simulation	1.2% on energy scale		
Jet energy scale and effect on p_T^{miss}	simulation	Shape, up to 10%		
p_T^{miss} energy scale	simulation	Shape, up to 11%		
Integrated luminosity	simulation	2.5%		
Norm. $W + \text{jets/QCD multijet}$	$W + \text{jets/QCD multijet}$	up to 20%		
Norm. $t\bar{t}$	$t\bar{t}$	6%		
Norm. diboson	Diboson	5%		
Norm. single top	Single top	5%		
Norm. SM Higgs boson	SM Higgs boson	up to 5%		
$Z + \text{jets}$ LO-NLO reweighting	$Z + \text{jets}$	Shape, up to 26%		
$W + \text{jets}$ NLO EW correction	$W + \text{jets}$	Shape, up to 6%		
WW NLO EW correction	WW	Shape, up to 12%		
ZZ NLO EW correction	ZZ	Shape, up to 2%		
Top quark p_T reweighting	$t\bar{t}$	Shape, up to 5%		
Theory: Higgs boson branching fraction	Signal + SM Higgs boson	1.7%		
Theory: renorm. and fact. scale	Signal	4%		
Theory: PDF	Signal	2%		
Limited number of events (bin-by-bin)	All processes	Shape only		

The hadronic τ_h efficiency is not fully correlated across all $\tau\tau$ final states because there are different discriminators used in each channel. The $\tau_h\tau_h$ channel has a 9% τ_h uncertainty due to a correlation with the $\tau_h\tau_h$ trigger systematic uncertainty. An uncertainty of 12% is assigned to simulated events containing an electron misidentified as a τ_h candidate, and 25% for a muon misidentified as a τ_h candidate [43]. A 2 (4)% uncertainty is assigned to the yield of multiboson and single top ($t\bar{t}$) processes to account for changes in overall normalization arising from uncertainties in the b tagging performance. Similarly, a 5% b tagging uncertainty is assigned to $Z + \text{jets}$ and SM Higgs boson processes, while all other processes, including signal, receive a 2% uncertainty. A systematic uncertainty of up to 20% is applied to QCD multijet background to account for yield differences in the same-sign CR. All of the background systematic uncertainties in the same-sign region are propagated to the total QCD multijet background uncertainty, which is taken to be 40%.

The $W + \text{jets}$ background has a p_T -dependent uncertainty, which approaches 10%, from predicted NLO EW K-factors where the full EW correction is treated as the systematic uncertainty [33–36]. Cross section uncertainties of the order of 5% are applied to the $t\bar{t}$ (6%), top quark (5%), and diboson (5%) processes [58–61]. In simulated $Z + \text{jets}$ samples, a shape uncertainty of 10% of the Z boson p_T reweighting correction, to account for higher-order effects, is used. The uncertainty in the $Z + \text{jets}$ background contribution is about 12% in the SR. The $t\bar{t}$ contribution includes a shape systematic uncertainty equivalent to 5% related to the top quark p_T spectrum, since there is evidence that the spectrum is softer in data than in simulation [61].

A 1.2% uncertainty in the τ lepton energy scale [43] is propagated through to the final signal extraction variables. The τ lepton energy scale depends on the τ_h decay mode and is correlated across all channels. A shape uncertainty is used for the uncertainty in the double τ_h trigger. A shift of 3% of the p_T of the trigger-level τ_h candidate leads to a 12% normalization difference at 40 GeV, and a 2% difference at 60 GeV. For $p_T > 60$ GeV, a constant 2% systematic uncertainty is applied.

To account for potentially different rates of jets misidentified as τ_h candidates between data and simulation, an uncertainty, applied as a function of the p_T of the τ_h candidate, is used for background events where the reconstructed τ_h candidate is matched to a jet at generator-level. The uncertainty increases to about 20% near a τ_h candidate $p_T = 200$ GeV, and acts to change the shape of the M_T^{tot} distribution. An asymmetric uncertainty related to the identification of τ_h with a high p_T is applied to signal and background simulation. The high- p_T τ_h efficiency measurement uses selected highly virtual W bosons and has limited statistical precision in comparison to the lower p_T $Z \rightarrow \tau\tau$ and $t\bar{t}$ τ_h efficiency studies. Therefore the asymmetric uncertainty is used in combination with a constant scale factor. It is proportional to p_T and has a value of +5% and −35% per 1 TeV. For the application of all of the aforementioned τ lepton uncertainties, simulated backgrounds are separated depending on whether the reconstructed τ_h candidates are matched to generated τ leptons.

In all simulated samples, uncertainties in the p_T^{miss} calculation related to unclustered energy deposits are taken into account. Uncertainties in the jet energy scale are included on an event-by-event basis and propagated to the p_T^{miss} calculation. Lastly, an uncertainty in the statistical precision of each process in each bin of the distribution is also included.

7 Results

The results of the analysis are derived from the maximum-likelihood fits presented in Sections 4 and 5 for the $h \rightarrow \gamma\gamma$ and $h \rightarrow \tau^+\tau^-$ channels, respectively.

7.1 Observed yields

For the $h \rightarrow \gamma\gamma$ channel, from the signal plus background fit to $m_{\gamma\gamma}$, the number of expected events from background processes are determined. The background yields and the observed number of events within 3 GeV of the SM Higgs boson mass are listed in Table 5 for both the low- and high- p_T^{miss} categories. The excess at low- p_T^{miss} has negligible effect on the results when combined with the high- p_T^{miss} category for the benchmark signals considered in this paper.

Table 5: Expected background yields and observed numbers of events for the $h \rightarrow \gamma\gamma$ channel in the $m_{\gamma\gamma}$ range of 122–128 GeV are shown for the low- and high- p_T^{miss} categories. The nonresonant background includes QCD multijet, $\gamma\gamma$, $\gamma + \text{jet}$, and EW backgrounds and is estimated from the analytic function fit to data. The SM Higgs boson background is presented separately for the irreducible Vh production and for the other production modes. For the resonant background contributions, both the statistical and the systematic uncertainties are listed. As detailed in Section 4.2, the systematic uncertainty associated with the nonresonant background is negligible.

Expected background	Low- p_T^{miss} category	High- p_T^{miss} category
SM $h \rightarrow \gamma\gamma$ (Vh)	2.9 ± 0.1 (stat) ± 0.2 (syst)	1.26 ± 0.05 (stat) ± 0.09 (syst)
SM $h \rightarrow \gamma\gamma$ (ggh, $t\bar{t}h$, VBF)	5.3 ± 0.3 (stat) ± 1.2 (syst)	0.11 ± 0.01 (stat) ± 0.01 (syst)
Nonresonant background	125.1 ± 11.2 (stat)	4.5 ± 2.1 (stat)
Total background	133 ± 11 (stat) ± 1 (syst)	5.9 ± 2.1 (stat) ± 0.1 (syst)
Observed events	159	6

In the $h \rightarrow \tau^+\tau^-$ channel, the final simultaneous fit to the M_T^{tot} distributions for the SR, and W + jets and QCD multijet CRs is performed in each of the three considered τ decay channels ($e\tau_h$, $\mu\tau_h$, and $\tau_h\tau_h$). The extracted post-fit yields for the expected number of background events and the number of events observed in data are shown in Table 6. The number of events observed is in good agreement with the number of events predicted by the SM backgrounds.

Table 6: Estimated background yields and observed numbers of events for $M_T^{\text{tot}} > 260$ GeV, in the SR of the $h \rightarrow \tau^+\tau^-$ channel. The uncertainties in the total expected yields include the statistical and systematic contributions.

Expected background	$e\tau_h$	$\mu\tau_h$	$\tau_h\tau_h$
W + jets/QCD multijet	13.1 ± 2.2	32.5 ± 6.2	3.8 ± 2.6
$t\bar{t}$	13.7 ± 1.6	24.8 ± 2.0	4.2 ± 1.3
SM Higgs boson	0.48 ± 0.08	0.72 ± 0.06	1.21 ± 0.08
Diboson	12.3 ± 1.0	21.5 ± 1.5	7.3 ± 0.6
$Z \rightarrow \tau\tau$	0.00 ± 0.01	0.0 ± 0.5	3.6 ± 1.2
$Z \rightarrow \ell\ell$	0.9 ± 1.9	2.0 ± 1.3	—
$Z \rightarrow \nu\nu$	—	—	0.4 ± 0.3
Total background	40.5 ± 3.3	81.8 ± 6.3	20.5 ± 3.0
Observed events	38	81	26

Aside from the small excess in the low- p_T^{miss} category of the $h \rightarrow \gamma\gamma$ channel, the observed numbers of events are consistent with SM expectations. All of the results presented here are interpreted in terms of the two benchmark models of DM production mentioned earlier. Expected signal yields and the product of the predicted signal acceptances and their efficiencies ($A\epsilon$) are summarized in Table 7 for selected mass points, in both $h \rightarrow \gamma\gamma$ and $h \rightarrow \tau^+\tau^-$ channels.

Table 7: The expected signal yields and the product of acceptance and efficiency ($A\epsilon$) for the two benchmark models. The Z' -2HDM signal is shown for the parameters $m_A = 300$ GeV and $m_{Z'} = 1000$ GeV, and the baryonic Z' signal, for the parameters $m_{DM} = 1$ GeV and $m_{Z'} = 10$ GeV.

Signal	$h \rightarrow \gamma\gamma$ channel		$h \rightarrow \tau^+\tau^-$ channel		
	Low- p_T^{miss}	High- p_T^{miss}	$e\tau_h$	$\mu\tau_h$	$\tau_h\tau_h$
Z'-2HDM					
Expected yield	0.1 ± 0.4	4.5 ± 0.6	6.5 ± 0.3	11.1 ± 0.5	14.3 ± 1.2
$A\epsilon$ [%]	0.1	42.6	2.2	3.6	4.4
Baryonic Z'					
Expected yield	12.3 ± 5.4	13.0 ± 5.6	8.2 ± 0.3	15.1 ± 0.6	18.1 ± 0.9
$A\epsilon$ [%]	6.6	7.0	0.2	0.3	0.3

A discussion of the results for the Z' -2HDM interpretation is presented in Section 7.2. The results in the context of the baryonic Z' interpretation are given in Section 7.3. The baryonic Z' results are also reinterpreted for comparison with direct detection experiments in Section 7.4 by looking at simplified DM models proposed by the ATLAS-CMS Dark Matter Forum [14].

7.2 Interpretation in the Z' -2HDM model

For the event selection given in Sections 4 and 5, the results interpreted in terms of the Z' -2HDM associated production of DM and a Higgs boson are presented here. The expected and observed yields are used to calculate an upper limit on the production cross section of DM+ h production via the Z' -2HDM mechanism. Upper limits are computed [62] at 95% confidence level (CL) using a profile likelihood ratio and the modified frequentist criterion [63, 64] with an asymptotic approximation [65]. The upper limits are obtained for each Higgs boson decay channel separately and for the statistical combination of the two. The two decay channels are combined using the Higgs boson branching fractions predicted by the SM [56]. In the combination of the two analyses, the theoretical uncertainties in the Higgs boson cross section and the systematic uncertainty in the integrated luminosity are assumed to be fully correlated between the two decay channels.

Figure 5 shows the 95% CL expected and observed upper limits on the DM production cross section ($\sigma_{95\%CL}$) as a function of Z' mass. Both the $h \rightarrow \gamma\gamma$ and $h \rightarrow \tau^+\tau^-$ channels, as well as the combination of the two, are shown for $m_A = 300$ GeV. These upper limits, although obtained with a DM mass of 100 GeV, can be considered valid for any DM mass below 100 GeV since the branching fraction for decays of A to DM particles decreases as the dark matter mass increases. The theoretical cross section (σ_{th}) is calculated with $m_{DM} = 100$ GeV, $g_{Z'} = 0.8$, and $g_{DM} = \tan\beta = 1$, as mentioned in Section 1.

To produce exclusion limits in the two-dimensional plane of Z' mass and A mass, an interpolation is performed. Fully simulated signal samples (mentioned in Section 3) were generated in a coarse grid of m_A and $m_{Z'}$. For the $h \rightarrow \gamma\gamma$ channel, the $m_{\gamma\gamma}$ shape does not depend on the mass of these particles, only the expected yield is affected by these masses. Therefore, the product $A\epsilon$ of the fully simulated samples is parametrized and used to extract the expected number of events for intermediate mass points. In the $h \rightarrow \tau^+\tau^-$ channel, this is not sufficient because the M_T^{tot} shape does depend on the particle masses. A reweighting technique is used to extract the yields for the intermediate mass points. Simulation samples were produced at generator-level for $m_{Z'}$ between 450 and 2000 GeV in steps of 50 GeV and for m_A between 300 and 700 GeV in steps of 25 GeV. These are compared with the full-simulation samples at generator-level. The bin-by-bin ratio of the SM-like Higgs boson p_T between the two samples is used to weight the full-simulation samples. This method was validated by applying the same procedure at the

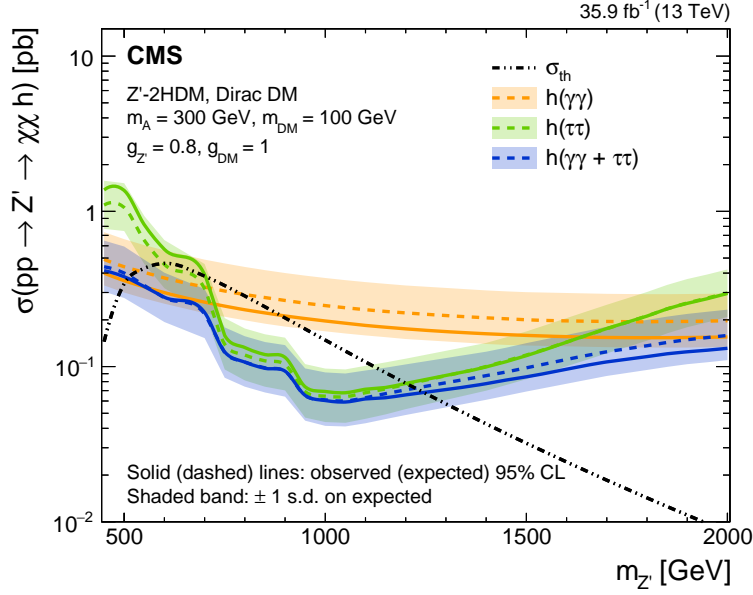


Figure 5: Expected and observed 95% CL upper limits on the Z' -2HDM cross section for dark matter associated production with a Higgs boson ($Z' \rightarrow \chi\chi h$) are shown. Limits are given for the $h \rightarrow \gamma\gamma$ channel, $h \rightarrow \tau^+\tau^-$ channel, and their combined exclusion.

generator-level among the samples for which full-simulation is available.

The interpolation between mass points is improved using kernel algorithms to display smooth, continuous exclusion contours. The resulting two-dimensional exclusion for the Z' -2HDM signal is shown in Fig. 6. The 95% CL expected and observed upper limits on signal strength ($\sigma_{95\% \text{ CL}}/\sigma_{\text{th}}$) are shown. Regions of the parameter space with $\sigma_{95\% \text{ CL}}/\sigma_{\text{th}} < 1$ are excluded at 95% CL under the nominal σ_{th} hypothesis. For $m_A = 300$ GeV, the $h \rightarrow \gamma\gamma$ channel alone excludes at 95% CL Z' masses up to 860 GeV, while the $h \rightarrow \tau^+\tau^-$ channel excludes $m_{Z'}$ up to 1200 GeV. The combination of these two decay channels excludes Z' masses up to 1265 GeV for $m_A = 300$ GeV. The Z' mass range considered is extended from previous CMS searches to include $450 \leq m_{Z'} < 600$ GeV.

7.3 Baryonic Z' model interpretation

Here the results presented in Section 7.1 are interpreted in the context of the baryonic Z' model. This paper presents the first baryonic Z' model interpretation of $h + p_{\text{T}}^{\text{miss}}$ searches with the CMS detector. The 95% CL upper limits on DM+ h cross section are calculated for the baryonic Z' production mechanism. The upper limits for each decay channel and the combination of the two channels are shown in Fig. 7. The σ_{th} is calculated assuming the choice of parameters detailed in Section 1. Results in the two-dimensional plane of m_{DM} and $m_{Z'}$ are produced using an interpolated grid produced in the same way as described in Section 7.2. The two-dimensional exclusion for this model is shown in Fig. 8, where the 95% CL upper limits on the signal strength are shown for each decay channel and for the combination of the $h \rightarrow \gamma\gamma$ and $h \rightarrow \tau^+\tau^-$ channels. For $m_{\text{DM}} = 1$ GeV, the $h \rightarrow \gamma\gamma$ channel excludes $m_{Z'}$ masses up to 574 GeV. The $h \rightarrow \tau^+\tau^-$ channel similarly excludes $m_{Z'}$ masses up to 450 GeV. The combination of the two decay channels excludes $m_{Z'}$ up to 615 GeV for $m_{\text{DM}} = 1$ GeV.

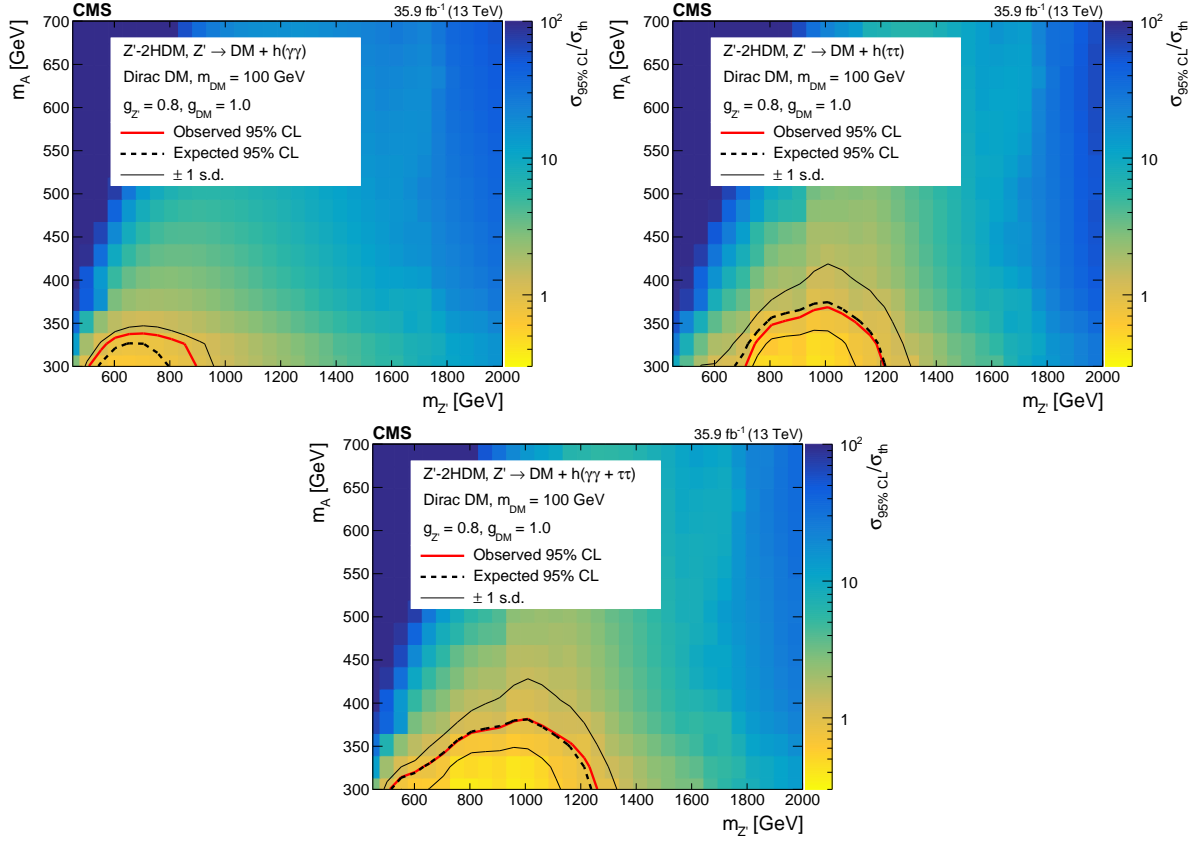


Figure 6: Observed 95% CL upper limits on the Z' -2HDM signal strength for the $h \rightarrow \gamma\gamma$ (left), $h \rightarrow \tau^+\tau^-$ (right), and combination of the two channels (lower center). The observed (expected) two-dimensional exclusion curves are shown with thick red (dashed black) lines. The plus and minus one standard deviation expected exclusion curves are also shown as thin black lines. The region below the lines is excluded.

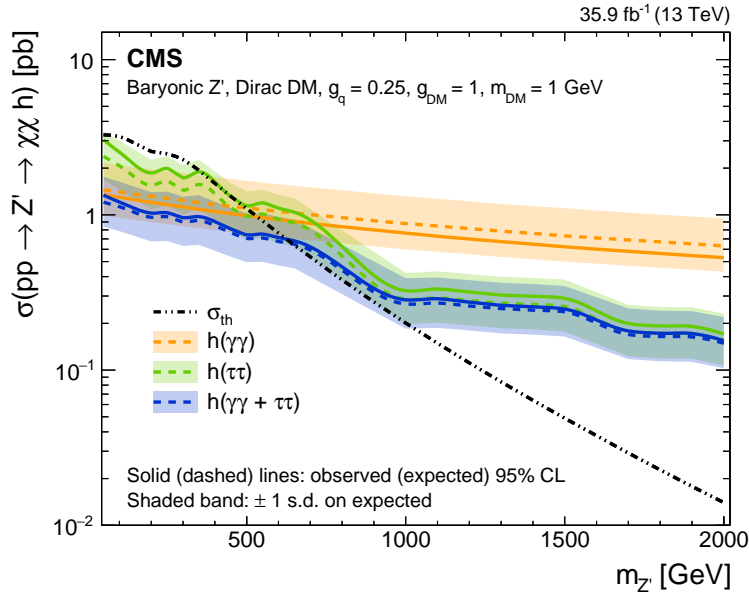


Figure 7: Expected and observed 95% CL upper limits on the baryonic Z' cross section for dark matter associated production with a Higgs boson ($Z' \rightarrow \chi\chi h$) are shown. Limits are given for the $h \rightarrow \gamma\gamma$ channel, $h \rightarrow \tau^+\tau^-$ channel, and their combined exclusion.

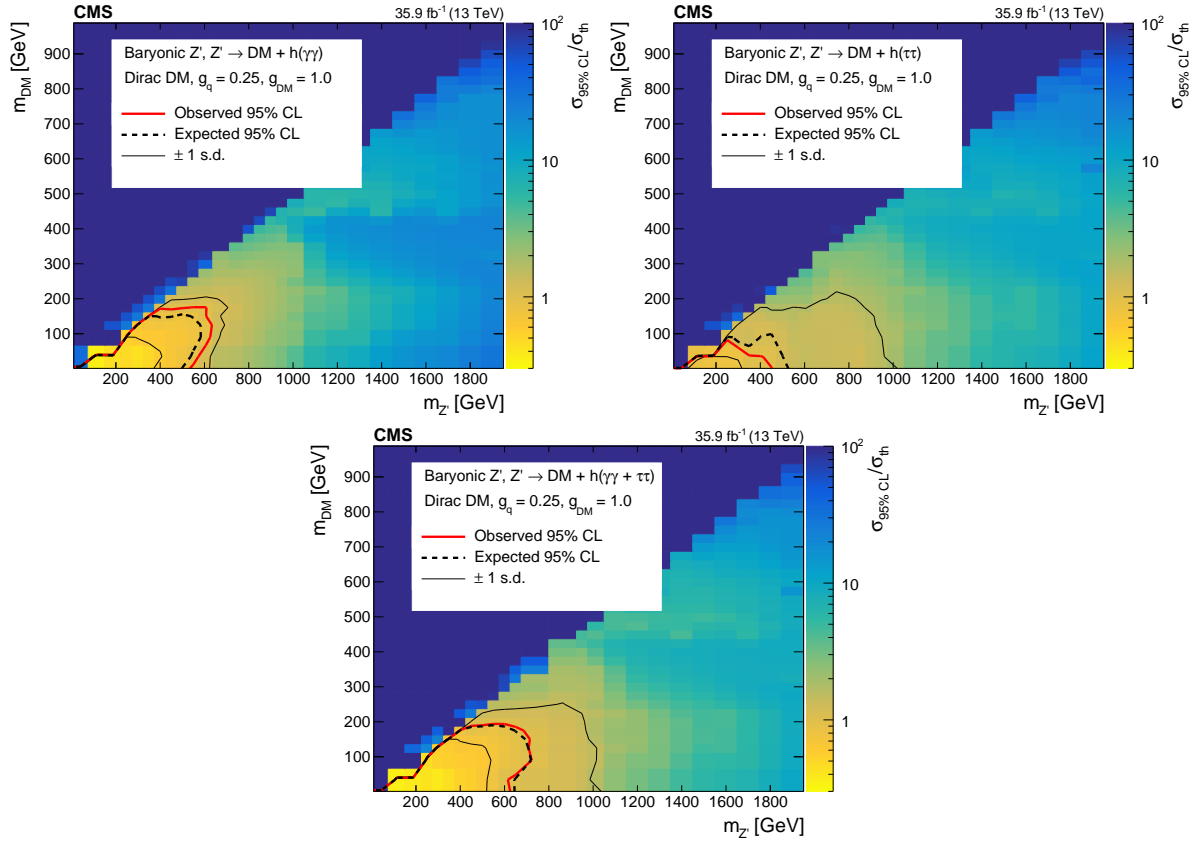


Figure 8: Observed 95% CL upper limits on the baryonic Z' signal strength for the $h \rightarrow \gamma\gamma$ (left), $h \rightarrow \tau^+\tau^-$ (right), and combination of the two channels (lower center). The observed (expected) two-dimensional exclusion curves are shown with thick red (dashed black) lines. The plus and minus one standard deviation expected exclusion curves are also shown as thin black lines. The region below the lines is excluded.

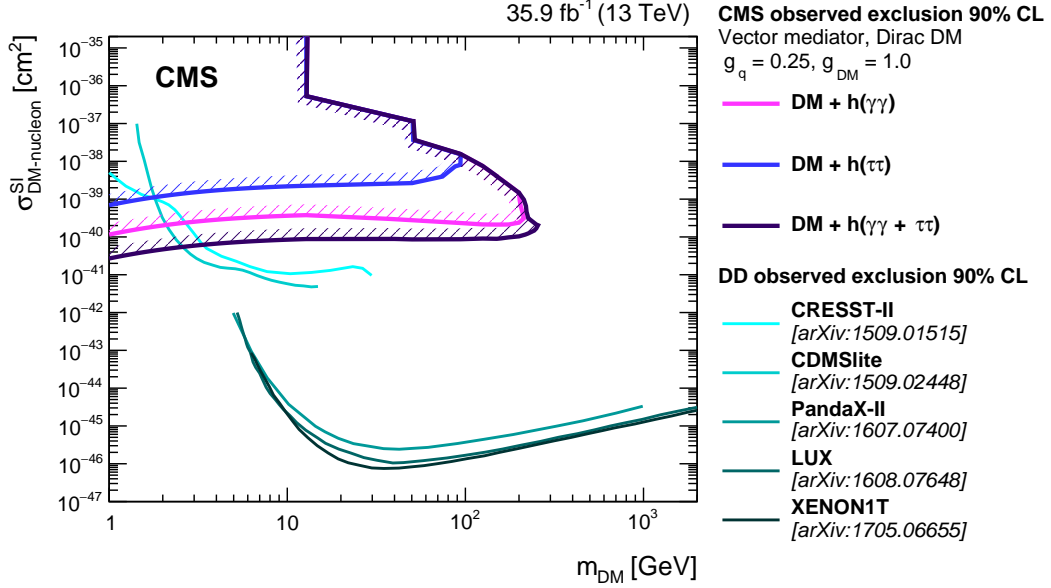


Figure 9: The 90% CL exclusion limits on the DM-nucleon SI scattering cross section as a function of m_{DM} . Results obtained in this analysis are compared with those from a selection of direct detection (DD) experiments. The latter exclude the regions above the curves. Limits from CDMSlite [66], LUX [67], XENON-1T [68], PandaX-II [69], and CRESST-II [70] are shown.

7.4 Simplified DM model interpretation

Limits from the baryonic Z' model are reinterpreted to infer limits on the s -channel simplified DM models that were proposed by the ATLAS-CMS Dark Matter Forum [14] for comparison with direct detection experiments. In the model considered in this analysis, Dirac DM particles couple to a vector mediator, which in turn couples to the SM quarks. A point in the parameter space of this model is determined by four variables: the DM particle mass m_{DM} , the mediator mass m_{med} , the mediator-DM coupling g_{DM} , and the universal mediator-quark coupling g_q . The couplings for this analysis are fixed to $g_{\text{DM}} = 1.0$ and $g_q = 0.25$, following the recommendation of Ref. [17].

The results are interpreted in the spin-independent (SI) cross section σ^{SI} for DM scattering off a nucleus. The value of σ^{SI} for a given point in the s -channel simplified DM model is determined by the equation [17]:

$$\sigma^{\text{SI}} = \frac{f^2(g_q)g_{\text{DM}}^2\mu_{\text{nDM}}^2}{\pi m_{\text{med}}^4}, \quad (3)$$

where μ_{nDM} is the reduced mass of the DM-nucleon system and $f(g_q)$ is the mediator-nucleon coupling, which is dependent on g_q . The resulting σ^{SI} limits as a function of DM mass are shown in Fig. 9. In the same plot, exclusions from several direct detection experiments are shown. For the baryonic Z' model, the limits are more stringent than direct detection experiments for $m_{\text{DM}} < 2.5$ GeV.

8 Summary

A search for dark matter particles produced in association with a Higgs boson has been performed. The study focuses on the case where the 125 GeV Higgs boson decays to either two photons or two τ leptons. This analysis is based on proton-proton collision data collected with

the CMS detector during 2016 at $\sqrt{s} = 13$ TeV, corresponding to an integrated luminosity of 35.9 fb^{-1} . The results of the search are interpreted in terms of a Z' -two-Higgs-doublet model (Z' -2HDM) and a baryonic Z' simplified model of dark matter production.

A statistical combination of the two channels was performed and these results were used to produce upper limits on dark matter production. Limits on the signal production cross section are calculated for both simplified models. For the Z' -2HDM signal, with an intermediate pseudoscalar of mass $m_A = 300$ GeV and $m_{\text{DM}} = 100$ GeV, Z' masses up to 1265 GeV are excluded at 95% confidence level. For the baryonic Z' model, with $m_{\text{DM}} = 1$ GeV, Z' masses up to 615 GeV are excluded. This is the first search for dark matter produced in association with a Higgs boson decaying to two τ leptons and the first to combine results from the $\gamma\gamma$ and $\tau^+\tau^-$ decay channels. The Z' -2HDM interpretation extended the Z' mass range compared with previous CMS searches. The interpretation of the results include the first baryonic Z' model interpretation for CMS and an extrapolation to limits on the spin-independent cross section for the dark matter-nucleon interaction.

Acknowledgments

We congratulate our colleagues in the CERN accelerator departments for the excellent performance of the LHC and thank the technical and administrative staffs at CERN and at other CMS institutes for their contributions to the success of the CMS effort. In addition, we gratefully acknowledge the computing centers and personnel of the Worldwide LHC Computing Grid for delivering so effectively the computing infrastructure essential to our analyses. Finally, we acknowledge the enduring support for the construction and operation of the LHC and the CMS detector provided by the following funding agencies: BMWFW and FWF (Austria); FNRS and FWO (Belgium); CNPq, CAPES, FAPERJ, FAPERGS, and FAPESP (Brazil); MES (Bulgaria); CERN; CAS, MoST, and NSFC (China); COLCIENCIAS (Colombia); MSES and CSF (Croatia); RPF (Cyprus); SENESCYT (Ecuador); MoER, ERC IUT, and ERDF (Estonia); Academy of Finland, MEC, and HIP (Finland); CEA and CNRS/IN2P3 (France); BMBF, DFG, and HGF (Germany); GSRT (Greece); NKFI (Hungary); DAE and DST (India); IPM (Iran); SFI (Ireland); INFN (Italy); MSIP and NRF (Republic of Korea); LAS (Lithuania); MOE and UM (Malaysia); BUAP, CINVESTAV, CONACYT, LNS, SEP, and UASLP-FAI (Mexico); MBIE (New Zealand); PAEC (Pakistan); MSHE and NSC (Poland); FCT (Portugal); JINR (Dubna); MON, RosAtom, RAS, RFBR, and NRC KI (Russia); MESTD (Serbia); SEIDI, CPAN, PCTI, and FEDER (Spain); Swiss Funding Agencies (Switzerland); MST (Taipei); ThEPCenter, IPST, STAR, and NSTDA (Thailand); TUBITAK and TAEK (Turkey); NASU and SFFR (Ukraine); STFC (United Kingdom); DOE and NSF (USA).

Individuals have received support from the Marie-Curie program and the European Research Council and Horizon 2020 Grant, contract No. 675440 (European Union); the Leventis Foundation; the A. P. Sloan Foundation; the Alexander von Humboldt Foundation; the Belgian Federal Science Policy Office; the Fonds pour la Formation à la Recherche dans l'Industrie et dans l'Agriculture (FRIA-Belgium); the Agentschap voor Innovatie door Wetenschap en Technologie (IWT-Belgium); the F.R.S.-FNRS and FWO (Belgium) under the "Excellence of Science - EOS" - be.h project n. 30820817; the Ministry of Education, Youth and Sports (MEYS) of the Czech Republic; the Lendület ("Momentum") Program and the János Bolyai Research Scholarship of the Hungarian Academy of Sciences, the New National Excellence Program ÚNKP, the NKFI research grants 123842, 123959, 124845, 124850 and 125105 (Hungary); the Council of Science and Industrial Research, India; the HOMING PLUS program of the Foundation for Polish Science, cofinanced from European Union, Regional Development Fund, the Mobility Plus program of

the Ministry of Science and Higher Education, the National Science Center (Poland), contracts Harmonia 2014/14/M/ST2/00428, Opus 2014/13/B/ST2/02543, 2014/15/B/ST2/03998, and 2015/19/B/ST2/02861, Sonata-bis 2012/07/E/ST2/01406; the National Priorities Research Program by Qatar National Research Fund; the Programa Estatal de Fomento de la Investigación Científica y Técnica de Excelencia María de Maeztu, grant MDM-2015-0509 and the Programa Severo Ochoa del Principado de Asturias; the Thalís and Aristeia programs cofinanced by EU-ESF and the Greek NSRF; the Rachadapisek Sompot Fund for Postdoctoral Fellowship, Chulalongkorn University and the Chulalongkorn Academic into Its 2nd Century Project Advancement Project (Thailand); the Welch Foundation, contract C-1845; and the Weston Havens Foundation (USA).

References

- [1] Planck Collaboration, “Planck 2015 results. XIII. Cosmological parameters”, *Astron. Astrophys.* **594** (2016) A13, doi:10.1051/0004-6361/201525830, arXiv:1502.01589.
- [2] G. Bertone, D. Hooper, and J. Silk, “Particle dark matter: evidence, candidates and constraints”, *Phys. Rept.* **405** (2005) 279, doi:10.1016/j.physrep.2004.08.031, arXiv:hep-ph/0404175.
- [3] ATLAS Collaboration, “Observation of a new particle in the search for the standard model Higgs boson with the ATLAS detector at the LHC”, *Phys. Lett. B* **716** (2012) 1, doi:10.1016/j.physletb.2012.08.020, arXiv:1207.7214.
- [4] CMS Collaboration, “Observation of a new boson at a mass of 125 GeV with the CMS experiment at the LHC”, *Phys. Lett. B* **716** (2012) 30, doi:10.1016/j.physletb.2012.08.021, arXiv:1207.7235.
- [5] CMS Collaboration, “Observation of a new boson with mass near 125 GeV in pp collisions at $\sqrt{s} = 7$ and 8 TeV”, *JHEP* **06** (2013) 081, doi:10.1007/JHEP06(2013)081, arXiv:1303.4571.
- [6] A. A. Petrov and W. Shepherd, “Searching for dark matter at LHC with mono-Higgs production”, *Phys. Lett. B* **730** (2014) 178, doi:10.1016/j.physletb.2014.01.051, arXiv:1311.1511.
- [7] A. Berlin, T. Lin, and L. Wang, “Mono-Higgs detection of dark matter at the LHC”, *JHEP* **78** (2014) 1, doi:10.1007/JHEP06(2014)078, arXiv:1402.7074.
- [8] L. Carpenter et al., “Mono-Higgs-boson: A new collider probe of dark matter”, *Phys. Rev. D* **89** (2014) 24, doi:10.1103/PhysRevD.89.075017, arXiv:1312.2592.
- [9] ATLAS Collaboration, “Search for dark matter produced in association with a Higgs boson decaying to two bottom quarks in pp collisions at $\sqrt{s} = 8$ TeV with the ATLAS detector”, *Phys. Rev. D* **93** (2016) 47, doi:10.1103/PhysRevD.93.072007, arXiv:1510.06218.
- [10] ATLAS Collaboration, “Search for dark matter in events with missing transverse momentum and a Higgs boson decaying to two photons in pp collisions at $\sqrt{s} = 8$ TeV with the ATLAS detector”, *Phys. Rev. Lett.* **115** (2015) 131801, doi:10.1103/PhysRevLett.115.131801, arXiv:1506.01081.

- [11] ATLAS Collaboration, “Search for dark matter in association with a Higgs boson decaying to b -quarks in pp collisions at $\sqrt{s} = 13$ TeV with the ATLAS detector”, *Phys. Lett. B* **765** (2017) 11, doi:10.1016/j.physletb.2016.11.035, arXiv:1609.04572.
- [12] CMS Collaboration, “Search for associated production of dark matter with a Higgs boson decaying to $b\bar{b}$ or $\gamma\gamma$ at $\sqrt{s} = 13$ TeV”, *JHEP* **10** (2017) 180, doi:10.1007/JHEP10(2017)180, arXiv:1703.05236.
- [13] ATLAS Collaboration, “Search for dark matter in association with a Higgs boson decaying to two photons at $\sqrt{s} = 13$ TeV with the ATLAS detector”, *Phys. Rev. D* **96** (2017) 112004, doi:10.1103/PhysRevD.96.112004, arXiv:1706.03948.
- [14] D. Abercrombie et al., “Dark matter benchmark models for early LHC Run-2 searches: Report of the ATLAS/CMS Dark Matter Forum”, (2015). arXiv:1507.00966.
- [15] N. Craig, J. Galloway, and S. Thomas, “Searching for signs of the second Higgs doublet”, (2013). arXiv:1305.2424.
- [16] G. C. Branco et al., “Theory and phenomenology of two-Higgs-doublet models”, *Phys. Rept.* **516** (2012) 1, doi:10.1016/j.physrep.2012.02.002, arXiv:1106.0034.
- [17] A. Boveia et al., “Recommendations on presenting LHC searches for missing transverse energy signals using simplified s -channel models of dark matter”, (2016). arXiv:1603.04156.
- [18] CMS Collaboration, “The CMS experiment at the CERN LHC”, *JINST* **3** (2008) S08004, doi:10.1088/1748-0221/3/08/S08004.
- [19] CMS Collaboration, “The CMS trigger system”, *JINST* **12** (2017) P01020, doi:10.1088/1748-0221/12/01/P01020, arXiv:1609.02366.
- [20] CMS Collaboration, “Particle-flow reconstruction and global event description with the CMS detector”, *JINST* **12** (2017) P10003, doi:10.1088/1748-0221/12/10/P10003, arXiv:1706.04965.
- [21] M. Cacciari, G. P. Salam, and G. Soyez, “The anti- k_T jet clustering algorithm”, *JHEP* **04** (2008) 063, doi:10.1088/1126-6708/2008/04/063, arXiv:0802.1189.
- [22] M. Cacciari, G. P. Salam, and G. Soyez, “FastJet user manual”, *Eur. Phys. J. C* **72** (2012) 1896, doi:10.1140/epjc/s10052-012-1896-2, arXiv:1111.6097.
- [23] CMS Collaboration, “Performance of photon reconstruction and identification with the CMS detector in proton-proton collisions at $\sqrt{s} = 8$ TeV”, *JINST* **10** (2015) P08010, doi:10.1088/1748-0221/10/08/P08010, arXiv:1502.02702.
- [24] CMS Collaboration, “Performance of CMS muon reconstruction in pp collision events at $\sqrt{s} = 7$ TeV”, *JINST* **7** (2012) P10002, doi:10.1088/1748-0221/7/10/P10002, arXiv:1206.4071.
- [25] CMS Collaboration, “Reconstruction and identification of τ lepton decays to hadrons and ν_τ at CMS”, *JINST* **11** (2016) P01019, doi:10.1088/1748-0221/11/01/P01019, arXiv:1510.07488.

-
- [26] CMS Collaboration, “Identification of heavy-flavour jets with the CMS detector in pp collisions at 13 TeV”, *JINST* **13** (2018) P05011, doi:10.1088/1748-0221/13/05/P05011, arXiv:1712.07158.
- [27] CMS Collaboration, “Performance of the CMS missing transverse momentum reconstruction in pp data at $\sqrt{s} = 8$ TeV”, *JINST* **10** (2015) P02006, doi:10.1088/1748-0221/10/02/P02006, arXiv:1411.0511.
- [28] CMS Collaboration, “Performance of missing energy reconstruction in 13 TeV pp collision data using the CMS detector”, CMS Physics Analysis Summary CMS-PAS-JME-16-004, 2016.
- [29] J. Alwall et al., “The automated computation of tree-level and next-to-leading order differential cross sections, and their matching to parton shower simulations”, *JHEP* **07** (2014) 079, doi:10.1007/JHEP07(2014)079, arXiv:1405.0301.
- [30] T. Sjöstrand et al., “An introduction to PYTHIA 8.2”, *Comput. Phys. Commun.* **191** (2015) 159, doi:10.1016/j.cpc.2015.01.024, arXiv:1410.3012.
- [31] T. Gleisberg et al., “Event generation with SHERPA 1.1”, *JHEP* **02** (2009) 007, doi:10.1088/1126-6708/2009/02/007, arXiv:0811.4622.
- [32] J. Alwall et al., “Comparative study of various algorithms for the merging of parton showers and matrix elements in hadronic collisions”, *Eur. Phys. J. C* **53** (2008) 473, doi:10.1140/epjc/s10052-007-0490-5, arXiv:0706.2569.
- [33] CMS Collaboration, “Search for dark matter produced with an energetic jet or a hadronically decaying W or Z boson at $\sqrt{s} = 13$ TeV”, *JHEP* **07** (2017) 014, doi:10.1007/JHEP07(2017)014, arXiv:1703.01651.
- [34] J. H. Kuhn, A. Kulesza, S. Pozzorini, and M. Schulze, “Electroweak corrections to hadronic photon production at large transverse momenta”, *JHEP* **03** (2006) 059, doi:10.1088/1126-6708/2006/03/059, arXiv:hep-ph/0508253.
- [35] S. Kallweit et al., “NLO electroweak automation and precise predictions for W+multijet production at the LHC”, *JHEP* **04** (2015) 012, doi:10.1007/JHEP04(2015)012, arXiv:1412.5157.
- [36] S. Kallweit et al., “NLO QCD+EW predictions for V + jets including off-shell vector-boson decays and multijet merging”, *JHEP* **04** (2016) 021, doi:10.1007/JHEP04(2016)021, arXiv:1511.08692.
- [37] S. Frixione, P. Nason, and C. Oleari, “Matching NLO QCD computations with parton shower simulations: the POWHEG method”, *JHEP* **11** (2007) 070, doi:10.1088/1126-6708/2007/11/070, arXiv:0709.2092.
- [38] S. Alioli, P. Nason, C. Oleari, and E. Re, “A general framework for implementing NLO calculations in shower Monte Carlo programs: the POWHEG BOX”, *JHEP* **06** (2010) 043, doi:10.1007/JHEP06(2010)043, arXiv:1002.2581.
- [39] S. Alioli et al., “Jet pair production in POWHEG”, *JHEP* **04** (2011) 081, doi:10.1007/JHEP04(2011)081, arXiv:1012.3380.

- [40] S. Alioli, P. Nason, C. Oleari, and E. Re, “NLO Higgs boson production via gluon fusion matched with shower in POWHEG”, *JHEP* **04** (2009) 002, doi:10.1088/1126-6708/2009/04/002, arXiv:0812.0578.
- [41] P. Nason, “A new method for combining NLO QCD with shower Monte Carlo algorithms”, *JHEP* **11** (2004) 040, doi:10.1088/1126-6708/2004/11/040, arXiv:hep-ph/0409146.
- [42] R. Frederix and S. Frixione, “Merging meets matching in MC@NLO”, *JHEP* **12** (2012) 61, doi:10.1007/JHEP12(2012)061, arXiv:1209.6215.
- [43] CMS Collaboration, “Observation of the Higgs boson decay to a pair of τ leptons with the CMS detector”, *Phys. Lett. B* **779** (2018) 283, doi:10.1016/j.physletb.2018.02.004, arXiv:1708.00373.
- [44] NNPDF Collaboration, “Parton distributions for the LHC Run II”, *JHEP* **04** (2015) 040, doi:10.1007/JHEP04(2015)040, arXiv:1410.8849.
- [45] P. Skands, S. Carrazza, and J. Rojo, “Tuning PYTHIA 8.1: the Monash 2013 tune”, *Eur. Phys. J. C* **74** (2014) 3024, doi:10.1140/epjc/s10052-014-3024-y, arXiv:1404.5630.
- [46] CMS Collaboration, “Event generator tunes obtained from underlying event and multiparton scattering measurements”, *Eur. Phys. J. C* **76** (2016) 155, doi:10.1140/epjc/s10052-016-3988-x, arXiv:1512.00815.
- [47] GEANT4 Collaboration, “GEANT4—a simulation toolkit”, *Nucl. Instrum. Meth. A* **506** (2003) 250, doi:10.1016/S0168-9002(03)01368-8.
- [48] CMS Collaboration, “Measurements of inclusive W and Z cross sections in pp collisions at $\sqrt{s} = 7$ TeV”, *JHEP* **01** (2011) 080, doi:10.1007/JHEP01(2011)080, arXiv:1012.2466.
- [49] M. Cacciari and G. P. Salam, “Pileup subtraction using jet areas”, *Phys. Lett. B* **659** (2008) 119, doi:10.1016/j.physletb.2007.09.077, arXiv:0707.1378.
- [50] CMS Collaboration, “Measurements of Higgs boson properties in the diphoton decay channel in proton-proton collisions at $\sqrt{s} = 13$ TeV”, (2018). arXiv:1804.02716. Submitted to *JHEP*.
- [51] CMS Collaboration, “Search for dijet resonances in proton-proton collisions at $\sqrt{s} = 13$ TeV and constraints on dark matter and other models”, *Phys. Lett. B* **769** (2017) 520, doi:10.1016/j.physletb.2017.02.012, arXiv:1611.03568.
- [52] CMS Collaboration, “Search for high-mass diphoton resonances in proton-proton collisions at 13 TeV and combination with 8 TeV search”, *Phys. Lett. B* **767** (2017) 147, doi:10.1016/j.physletb.2017.01.027, arXiv:1609.02507.
- [53] CMS Collaboration, “Performance of tau-lepton reconstruction and identification in CMS”, *JINST* **7** (2012) P01001, doi:10.1088/1748-0221/7/01/P01001, arXiv:1109.6034.
- [54] CMS Collaboration, “CMS luminosity measurements for the 2016 data taking period”, CMS Physics Analysis Summary CMS-PAS-LUM-17-001, 2017.

-
- [55] J. Butterworth et al., “PDF4LHC recommendations for LHC Run II”, *J. Phys. G* **43** (2016) 023001, doi:10.1088/0954-3899/43/2/023001, arXiv:1510.03865.
- [56] D. de Florian et al., “Handbook of LHC Higgs cross sections: 4. deciphering the nature of the Higgs sector”, CERN Report CERN-2017-002-M, 2016.
doi:10.23731/CYRM-2017-002, arXiv:1610.07922.
- [57] CMS Collaboration, “Measurement of differential fiducial cross sections for Higgs boson production in the diphoton decay channel in pp collisions at $\sqrt{s} = 13$ TeV”, CMS Physics Analysis Summary CMS-PAS-HIG-17-015, 2017.
- [58] CMS Collaboration, “Cross section measurement of t -channel single top quark production in pp collisions at $\sqrt{s} = 13$ TeV”, *Phys. Lett. B* **772** (2017) 752,
doi:10.1016/j.physletb.2017.07.047, arXiv:1610.00678.
- [59] CMS Collaboration, “Measurement of the WZ production cross section in pp collisions at $\sqrt{s} = 13$ TeV”, *Phys. Lett. B* **766** (2017) 268,
doi:10.1016/j.physletb.2017.01.011, arXiv:1607.06943.
- [60] CMS Collaboration, “Measurements of the $pp \rightarrow ZZ$ production cross section and the $Z \rightarrow 4\ell$ branching fraction, and constraints on anomalous triple gauge couplings at $\sqrt{s} = 13$ TeV”, *Eur. Phys. J. C* **78** (2018) 165,
doi:10.1140/epjc/s10052-018-5567-9, arXiv:1709.08601.
- [61] CMS Collaboration, “Measurement of differential cross sections for top quark pair production using the lepton+jets final state in proton-proton collisions at 13 TeV”, *Phys. Rev. D* **95** (2017) 092001, doi:10.1103/PhysRevD.95.092001, arXiv:1610.04191.
- [62] The ATLAS Collaboration, The CMS Collaboration, The LHC Higgs Combination Group, “Procedure for the LHC Higgs boson search combination in Summer 2011”, Technical Report CMS-NOTE-2011-005. ATL-PHYS-PUB-2011-11, 2011.
- [63] T. Junk, “Confidence level computation for combining searches with small statistics”, *Nucl. Instrum. Meth. A* **434** (1999) 435, doi:10.1016/S0168-9002(99)00498-2, arXiv:hep-ex/9902006.
- [64] A. L. Read, “Presentation of search results: the CL_s technique”, *J. Phys. G* **28** (2002) 2693, doi:10.1088/0954-3899/28/10/313.
- [65] G. Cowan, K. Cranmer, E. Gross, and O. Vitells, “Asymptotic formulae for likelihood-based tests of new physics”, *Eur. Phys. J. C* **71** (2011) 1554,
doi:10.1140/epjc/s10052-011-1554-0, arXiv:1007.1727. [Erratum:
doi:10.1140/epjc/s10052-013-2501-z].
- [66] SuperCDMS Collaboration, “New results from the search for low-mass weakly interacting massive particles with the CDMS Low Ionization Threshold Experiment”, *Phys. Rev. Lett.* **116** (2016) 071301, doi:10.1103/PhysRevLett.116.071301, arXiv:1509.02448.
- [67] LUX Collaboration, “Results from a search for dark matter in the complete LUX exposure”, *Phys. Rev. Lett.* **118** (2017) 021303,
doi:10.1103/PhysRevLett.118.021303, arXiv:1608.07648.

-
- [68] XENON Collaboration, “First dark matter search results from the XENON1T experiment”, *Phys. Rev. Lett.* **119** (2017) 181301, doi:10.1103/PhysRevLett.119.181301, arXiv:1705.06655.
- [69] PandaX-II Collaboration, “Dark matter results from 54-ton-day exposure of PandaX-II experiment”, *Phys. Rev. Lett.* **119** (2017) 181302, doi:10.1103/PhysRevLett.119.181302, arXiv:1708.06917.
- [70] CRESST-II Collaboration, “Results on light dark matter particles with a low-threshold CRESST-II detector”, *Eur. Phys. J. C* **76** (2016) 25, doi:10.1140/epjc/s10052-016-3877-3, arXiv:1509.01515.

A The CMS Collaboration

Yerevan Physics Institute, Yerevan, Armenia

A.M. Sirunyan, A. Tumasyan

Institut für Hochenergiephysik, Wien, Austria

W. Adam, F. Ambrogio, E. Asilar, T. Bergauer, J. Brandstetter, M. Dragicevic, J. Erö, A. Escalante Del Valle, M. Flechl, R. Frühwirth¹, V.M. Ghete, J. Hrubec, M. Jeitler¹, N. Krammer, I. Krätschmer, D. Liko, T. Madlener, I. Mikulec, N. Rad, H. Rohringer, J. Schieck¹, R. Schöfbeck, M. Spanring, D. Spitzbart, A. Taurok, W. Waltenberger, J. Wittmann, C.-E. Wulz¹, M. Zarucki

Institute for Nuclear Problems, Minsk, Belarus

V. Chekhovsky, V. Mossolov, J. Suarez Gonzalez

Universiteit Antwerpen, Antwerpen, Belgium

E.A. De Wolf, D. Di Croce, X. Janssen, J. Lauwers, M. Pieters, M. Van De Klundert, H. Van Haevermaet, P. Van Mechelen, N. Van Remortel

Vrije Universiteit Brussel, Brussel, Belgium

S. Abu Zeid, F. Blekman, J. D'Hondt, I. De Bruyn, J. De Clercq, K. Deroover, G. Flouris, D. Lontkovskyi, S. Lowette, I. Marchesini, S. Moortgat, L. Moreels, Q. Python, K. Skovpen, S. Tavernier, W. Van Doninck, P. Van Mulders, I. Van Parijs

Université Libre de Bruxelles, Bruxelles, Belgium

D. Beghin, B. Bilin, H. Brun, B. Clerbaux, G. De Lentdecker, H. Delannoy, B. Dorney, G. Fasanella, L. Favart, R. Goldouzian, A. Grebenyuk, A.K. Kalsi, T. Lenzi, J. Luetic, N. Postiau, E. Starling, L. Thomas, C. Vander Velde, P. Vanlaer, D. Vannerom, Q. Wang

Ghent University, Ghent, Belgium

T. Cornelis, D. Dobur, A. Fagot, M. Gul, I. Khvastunov², D. Poyraz, C. Roskas, D. Trocino, M. Tytgat, W. Verbeke, B. Vermassen, M. Vit, N. Zaganidis

Université Catholique de Louvain, Louvain-la-Neuve, Belgium

H. Bakhshiansohi, O. Bondu, S. Brochet, G. Bruno, C. Caputo, P. David, C. Delaere, M. Delcourt, B. Francois, A. Giammanco, G. Krintiras, V. Lemaitre, A. Magitteri, A. Mertens, M. Musich, K. Piotrkowski, A. Saggio, M. Vidal Marono, S. Wertz, J. Zobec

Centro Brasileiro de Pesquisas Fisicas, Rio de Janeiro, Brazil

F.L. Alves, G.A. Alves, L. Brito, M. Correa Martins Junior, G. Correia Silva, C. Hensel, A. Moraes, M.E. Pol, P. Rebello Teles

Universidade do Estado do Rio de Janeiro, Rio de Janeiro, Brazil

E. Belchior Batista Das Chagas, W. Carvalho, J. Chinellato³, E. Coelho, E.M. Da Costa, G.G. Da Silveira⁴, D. De Jesus Damiao, C. De Oliveira Martins, S. Fonseca De Souza, H. Malbouisson, D. Matos Figueiredo, M. Melo De Almeida, C. Mora Herrera, L. Mundim, H. Nogima, W.L. Prado Da Silva, L.J. Sanchez Rosas, A. Santoro, A. Sznajder, M. Thiel, E.J. Tonelli Manganote³, F. Torres Da Silva De Araujo, A. Vilela Pereira

Universidade Estadual Paulista ^a, Universidade Federal do ABC ^b, São Paulo, Brazil

S. Ahuja^a, C.A. Bernardes^a, L. Calligaris^a, T.R. Fernandez Perez Tomei^a, E.M. Gregores^b, P.G. Mercadante^b, S.F. Novaes^a, SandraS. Padula^a, D. Romero Abad^b

Institute for Nuclear Research and Nuclear Energy, Bulgarian Academy of Sciences, Sofia,

Bulgaria

A. Aleksandrov, R. Hadjiiska, P. Iaydjiev, A. Marinov, M. Misheva, M. Rodozov, M. Shopova, G. Sultanov

University of Sofia, Sofia, Bulgaria

A. Dimitrov, L. Litov, B. Pavlov, P. Petkov

Beihang University, Beijing, China

W. Fang⁵, X. Gao⁵, L. Yuan

Institute of High Energy Physics, Beijing, China

M. Ahmad, J.G. Bian, G.M. Chen, H.S. Chen, M. Chen, Y. Chen, C.H. Jiang, D. Leggat, H. Liao, Z. Liu, F. Romeo, S.M. Shaheen⁶, A. Spiezia, J. Tao, C. Wang, Z. Wang, E. Yazgan, H. Zhang, J. Zhao

State Key Laboratory of Nuclear Physics and Technology, Peking University, Beijing, China

Y. Ban, G. Chen, A. Levin, J. Li, L. Li, Q. Li, Y. Mao, S.J. Qian, D. Wang, Z. Xu

Tsinghua University, Beijing, China

Y. Wang

Universidad de Los Andes, Bogota, Colombia

C. Avila, A. Cabrera, C.A. Carrillo Montoya, L.F. Chaparro Sierra, C. Florez, C.F. González Hernández, M.A. Segura Delgado

University of Split, Faculty of Electrical Engineering, Mechanical Engineering and Naval Architecture, Split, Croatia

B. Courbon, N. Godinovic, D. Lelas, I. Puljak, T. Sculac

University of Split, Faculty of Science, Split, Croatia

Z. Antunovic, M. Kovac

Institute Rudjer Boskovic, Zagreb, Croatia

V. Brigljevic, D. Ferencek, K. Kadija, B. Mesic, A. Starodumov⁷, T. Susa

University of Cyprus, Nicosia, Cyprus

M.W. Ather, A. Attikis, M. Kolosova, G. Mavromanolakis, J. Mousa, C. Nicolaou, F. Ptochos, P.A. Razis, H. Rykaczewski

Charles University, Prague, Czech Republic

M. Finger⁸, M. Finger Jr.⁸

Escuela Politecnica Nacional, Quito, Ecuador

E. Ayala

Universidad San Francisco de Quito, Quito, Ecuador

E. Carrera Jarrin

Academy of Scientific Research and Technology of the Arab Republic of Egypt, Egyptian Network of High Energy Physics, Cairo, Egypt

Y. Assran^{9,10}, S. Elgammal¹⁰, S. Khalil¹¹

National Institute of Chemical Physics and Biophysics, Tallinn, Estonia

S. Bhowmik, A. Carvalho Antunes De Oliveira, R.K. Dewanjee, K. Ehataht, M. Kadastik, M. Raidal, C. Veelken

Department of Physics, University of Helsinki, Helsinki, Finland

P. Eerola, H. Kirschenmann, J. Pekkanen, M. Voutilainen

Helsinki Institute of Physics, Helsinki, Finland

J. Havukainen, J.K. Heikkilä, T. Järvinen, V. Karimäki, R. Kinnunen, T. Lampén, K. Lassila-Perini, S. Laurila, S. Lehti, T. Lindén, P. Luukka, T. Mäenpää, H. Siikonen, E. Tuominen, J. Tuominiemi

Lappeenranta University of Technology, Lappeenranta, Finland

T. Tuuva

IRFU, CEA, Université Paris-Saclay, Gif-sur-Yvette, France

M. Besancon, F. Couderc, M. Dejardin, D. Denegri, J.L. Faure, F. Ferri, S. Ganjour, A. Givernaud, P. Gras, G. Hamel de Monchenault, P. Jarry, C. Leloup, E. Locci, J. Malcles, G. Negro, J. Rander, A. Rosowsky, M.Ö. Sahin, M. Titov

Laboratoire Leprince-Ringuet, Ecole polytechnique, CNRS/IN2P3, Université Paris-Saclay, Palaiseau, France

A. Abdulsalam¹², C. Amendola, I. Antropov, F. Beaudette, P. Busson, C. Charlot, R. Granier de Cassagnac, I. Kucher, S. Lisniak, A. Lobanov, J. Martin Blanco, M. Nguyen, C. Ochando, G. Ortona, P. Pigard, R. Salerno, J.B. Sauvan, Y. Sirois, A.G. Stahl Leiton, A. Zabi, A. Zghiche

Université de Strasbourg, CNRS, IPHC UMR 7178, Strasbourg, France

J.-L. Agram¹³, J. Andrea, D. Bloch, J.-M. Brom, E.C. Chabert, V. Cherepanov, C. Collard, E. Conte¹³, J.-C. Fontaine¹³, D. Gelé, U. Goerlach, M. Jansová, A.-C. Le Bihan, N. Tonon, P. Van Hove

Centre de Calcul de l'Institut National de Physique Nucleaire et de Physique des Particules, CNRS/IN2P3, Villeurbanne, France

S. Gadrat

Université de Lyon, Université Claude Bernard Lyon 1, CNRS-IN2P3, Institut de Physique Nucléaire de Lyon, Villeurbanne, France

S. Beauceron, C. Bernet, G. Boudoul, N. Chanon, R. Chierici, D. Contardo, P. Depasse, H. El Mamouni, J. Fay, L. Finco, S. Gascon, M. Gouzevitch, G. Grenier, B. Ille, F. Lagarde, I.B. Laktineh, H. Lattaud, M. Lethuillier, L. Mirabito, A.L. Pequegnot, S. Perries, A. Popov¹⁴, V. Sordini, M. Vander Donckt, S. Viret, S. Zhang

Georgian Technical University, Tbilisi, Georgia

A. Khvedelidze⁸

Tbilisi State University, Tbilisi, Georgia

Z. Tsamalaidze⁸

RWTH Aachen University, I. Physikalisches Institut, Aachen, Germany

C. Autermann, L. Feld, M.K. Kiesel, K. Klein, M. Lipinski, M. Preuten, M.P. Rauch, C. Schomakers, J. Schulz, M. Teroerde, B. Wittmer, V. Zhukov¹⁴

RWTH Aachen University, III. Physikalisches Institut A, Aachen, Germany

A. Albert, D. Duchardt, M. Endres, M. Erdmann, T. Esch, R. Fischer, S. Ghosh, A. Güth, T. Hebbeker, C. Heidemann, K. Hoepfner, H. Keller, S. Knutzen, L. Mastrolorenzo, M. Merschmeyer, A. Meyer, P. Millet, S. Mukherjee, T. Pook, M. Radziej, H. Reithler, M. Rieger, F. Scheuch, A. Schmidt, D. Teyssier

RWTH Aachen University, III. Physikalisches Institut B, Aachen, Germany

G. Flügge, O. Hlushchenko, B. Kargoll, T. Kress, A. Künsken, T. Müller, A. Nehr Korn, A. Nowack, C. Pistone, O. Pooth, H. Sert, A. Stahl¹⁵

Deutsches Elektronen-Synchrotron, Hamburg, Germany

M. Aldaya Martin, T. Arndt, C. Asawatangtrakuldee, I. Babounikau, K. Beernaert, O. Behnke, U. Behrens, A. Bermúdez Martínez, D. Bertsche, A.A. Bin Anuar, K. Borras¹⁶, V. Botta, A. Campbell, P. Connor, C. Contreras-Campana, F. Costanza, V. Danilov, A. De Wit, M.M. Defranchis, C. Diez Pardos, D. Domínguez Damiani, G. Eckerlin, T. Eichhorn, A. Elwood, E. Eren, E. Gallo¹⁷, A. Geiser, J.M. Grados Luyando, A. Grohsjean, P. Gunnellini, M. Guthoff, M. Haranko, A. Harb, J. Hauk, H. Jung, M. Kasemann, J. Keaveney, C. Kleinwort, J. Knolle, D. Krücker, W. Lange, A. Lelek, T. Lenz, K. Lipka, W. Lohmann¹⁸, R. Mankel, I.-A. Melzer-Pellmann, A.B. Meyer, M. Meyer, M. Missiroli, G. Mittag, J. Mnich, V. Myronenko, S.K. Pflitsch, D. Pitzl, A. Raspereza, M. Savitskyi, P. Saxena, P. Schütze, C. Schwanenberger, R. Shevchenko, A. Singh, N. Stefaniuk, H. Tholen, O. Turkot, A. Vagnerini, G.P. Van Onsem, R. Walsh, Y. Wen, K. Wichmann, C. Wissing, O. Zenaiev

University of Hamburg, Hamburg, Germany

R. Aggleton, S. Bein, L. Benato, A. Benecke, V. Blobel, M. Centis Vignali, T. Dreyer, E. Garutti, D. Gonzalez, J. Haller, A. Hinemann, A. Karavdina, G. Kasieczka, R. Klanner, R. Kogler, N. Kovalchuk, S. Kurz, V. Kutzner, J. Lange, D. Marconi, J. Multhaup, M. Niedziela, D. Nowatschin, A. Perieanu, A. Reimers, O. Rieger, C. Scharf, P. Schleper, S. Schumann, J. Schwandt, J. Sonneveld, H. Stadie, G. Steinbrück, F.M. Stober, M. Stöver, D. Troendle, A. Vanhoefer, B. Vormwald

Karlsruher Institut fuer Technology

M. Akbiyik, C. Barth, M. Baselga, S. Baur, E. Butz, R. Caspart, T. Chwalek, F. Colombo, W. De Boer, A. Dierlamm, N. Faltermann, B. Freund, M. Giffels, M.A. Harrendorf, F. Hartmann¹⁵, S.M. Heindl, U. Husemann, F. Kassel¹⁵, I. Katkov¹⁴, S. Kudella, H. Mildner, S. Mitra, M.U. Mozer, Th. Müller, M. Plagge, G. Quast, K. Rabbertz, M. Schröder, I. Shvetsov, G. Sieber, H.J. Simonis, R. Ulrich, S. Wayand, M. Weber, T. Weiler, S. Williamson, C. Wöhrmann, R. Wolf

Institute of Nuclear and Particle Physics (INPP), NCSR Demokritos, Aghia Paraskevi, Greece

G. Anagnostou, G. Daskalakis, T. Gerasis, A. Kyriakis, D. Loukas, G. Paspalaki, I. Topsis-Giotis

National and Kapodistrian University of Athens, Athens, Greece

G. Karathanasis, S. Kesisoglou, P. Kontaxakis, A. Panagiotou, N. Saoulidou, E. Tziaferi, K. Vellidis

National Technical University of Athens, Athens, Greece

K. Kousouris, I. Papakrivopoulos, G. Tsipolitis

University of Ioánnina, Ioánnina, Greece

I. Evangelou, C. Foudas, P. Giannios, P. Katsoulis, P. Kokkas, S. Mallios, N. Manthos, I. Papadopoulos, E. Paradas, J. Strologas, F.A. Triantis, D. Tsitsonis

MTA-ELTE Lendület CMS Particle and Nuclear Physics Group, Eötvös Loránd University, Budapest, Hungary

M. Bartók¹⁹, M. Csanad, N. Filipovic, P. Major, M.I. Nagy, G. Pasztor, O. Surányi, G.I. Veres

Wigner Research Centre for Physics, Budapest, Hungary

G. Bencze, C. Hajdu, D. Horvath²⁰, Á. Hunyadi, F. Sikler, T.Á. Vámi, V. Veszpremi, G. Vesztergombi[†]

Institute of Nuclear Research ATOMKI, Debrecen, Hungary

N. Beni, S. Czellar, J. Karancsi²¹, A. Makovec, J. Molnar, Z. Szillasi

Institute of Physics, University of Debrecen, Debrecen, Hungary

P. Raics, Z.L. Trocsanyi, B. Ujvari

Indian Institute of Science (IISc), Bangalore, India

S. Choudhury, J.R. Komaragiri, P.C. Tiwari

National Institute of Science Education and Research, HBNI, Bhubaneswar, India

S. Bahinipati²², C. Kar, P. Mal, K. Mandal, A. Nayak²³, D.K. Sahoo²², S.K. Swain

Panjab University, Chandigarh, India

S. Bansal, S.B. Beri, V. Bhatnagar, S. Chauhan, R. Chawla, N. Dhingra, R. Gupta, A. Kaur, A. Kaur, M. Kaur, S. Kaur, R. Kumar, P. Kumari, M. Lohan, A. Mehta, K. Sandeep, S. Sharma, J.B. Singh, G. Walia

University of Delhi, Delhi, India

A. Bhardwaj, B.C. Choudhary, R.B. Garg, M. Gola, S. Keshri, Ashok Kumar, S. Malhotra, M. Naimuddin, P. Priyanka, K. Ranjan, Aashaq Shah, R. Sharma

Saha Institute of Nuclear Physics, HBNI, Kolkata, India

R. Bhardwaj²⁴, M. Bharti, R. Bhattacharya, S. Bhattacharya, U. Bhawandeep²⁴, D. Bhowmik, S. Dey, S. Dutt²⁴, S. Dutta, S. Ghosh, K. Mondal, S. Nandan, A. Purohit, P.K. Rout, A. Roy, S. Roy Chowdhury, S. Sarkar, M. Sharan, B. Singh, S. Thakur²⁴

Indian Institute of Technology Madras, Madras, India

P.K. Behera

Bhabha Atomic Research Centre, Mumbai, India

R. Chudasama, D. Dutta, V. Jha, V. Kumar, P.K. Netrakanti, L.M. Pant, P. Shukla

Tata Institute of Fundamental Research-A, Mumbai, India

T. Aziz, M.A. Bhat, S. Dugad, G.B. Mohanty, N. Sur, B. Sutar, RavindraKumar Verma

Tata Institute of Fundamental Research-B, Mumbai, India

S. Banerjee, S. Bhattacharya, S. Chatterjee, P. Das, M. Guchait, Sa. Jain, S. Karmakar, S. Kumar, M. Maity²⁵, G. Majumder, K. Mazumdar, N. Sahoo, T. Sarkar²⁵

Indian Institute of Science Education and Research (IISER), Pune, India

S. Chauhan, S. Dube, V. Hegde, A. Kapoor, K. Kothekar, S. Pandey, A. Rane, S. Sharma

Institute for Research in Fundamental Sciences (IPM), Tehran, Iran

S. Chenarani²⁶, E. Eskandari Tadavani, S.M. Etesami²⁶, M. Khakzad, M. Mohammadi Najafabadi, M. Naseri, F. Rezaei Hosseinabadi, B. Safarzadeh²⁷, M. Zeinali

University College Dublin, Dublin, Ireland

M. Felcini, M. Grunewald

INFN Sezione di Bari ^a, Università di Bari ^b, Politecnico di Bari ^c, Bari, Italy

M. Abbrescia^{a,b}, C. Calabria^{a,b}, A. Colaleo^a, D. Creanza^{a,c}, L. Cristella^{a,b}, N. De Filippis^{a,c}, M. De Palma^{a,b}, A. Di Florio^{a,b}, F. Errico^{a,b}, L. Fiore^a, A. Gelmi^{a,b}, G. Iaselli^{a,c}, M. Ince^{a,b}, S. Lezki^{a,b}, G. Maggi^{a,c}, M. Maggi^a, G. Miniello^{a,b}, S. My^{a,b}, S. Nuzzo^{a,b}, A. Pompili^{a,b}, G. Pugliese^{a,c}, R. Radogna^a, A. Ranieri^a, G. Selvaggi^{a,b}, A. Sharma^a, L. Silvestris^a, R. Venditti^a, P. Verwilligen^a, G. Zito^a

INFN Sezione di Bologna ^a, Università di Bologna ^b, Bologna, Italy

G. Abbiendi^a, C. Battilana^{a,b}, D. Bonacorsi^{a,b}, L. Borgonovi^{a,b}, S. Braibant-Giacomelli^{a,b}, R. Campanini^{a,b}, P. Capiluppi^{a,b}, A. Castro^{a,b}, F.R. Cavallo^a, S.S. Chhibra^{a,b}, C. Ciocca^a, G. Codispoti^{a,b}, M. Cuffiani^{a,b}, G.M. Dallavalle^a, F. Fabbri^a, A. Fanfani^{a,b}, P. Giacomelli^a, C. Grandi^a, L. Guiducci^{a,b}, F. Iemmi^{a,b}, S. Marcellini^a, G. Masetti^a, A. Montanari^a, F.L. Navarria^{a,b}, A. Perrotta^a, F. Primavera^{a,b,15}, A.M. Rossi^{a,b}, T. Rovelli^{a,b}, G.P. Siroli^{a,b}, N. Tosi^a

INFN Sezione di Catania ^a, Università di Catania ^b, Catania, Italy

S. Albergo^{a,b}, A. Di Mattia^a, R. Potenza^{a,b}, A. Tricomi^{a,b}, C. Tuve^{a,b}

INFN Sezione di Firenze ^a, Università di Firenze ^b, Firenze, Italy

G. Barbagli^a, K. Chatterjee^{a,b}, V. Ciulli^{a,b}, C. Civinini^a, R. D'Alessandro^{a,b}, E. Focardi^{a,b}, G. Latino^a, P. Lenzi^{a,b}, M. Meschini^a, S. Paoletti^a, L. Russo^{a,28}, G. Sguazzoni^a, D. Strom^a, L. Viliani^a

INFN Laboratori Nazionali di Frascati, Frascati, Italy

L. Benussi, S. Bianco, F. Fabbri, D. Piccolo

INFN Sezione di Genova ^a, Università di Genova ^b, Genova, Italy

F. Ferro^a, F. Ravera^{a,b}, E. Robutti^a, S. Tosi^{a,b}

INFN Sezione di Milano-Bicocca ^a, Università di Milano-Bicocca ^b, Milano, Italy

A. Benaglia^a, A. Beschi^b, L. Brianza^{a,b}, F. Brivio^{a,b}, V. Ciriolo^{a,b,15}, S. Di Guida^{a,d,15}, M.E. Dinardo^{a,b}, S. Fiorendi^{a,b}, S. Gennai^a, A. Ghezzi^{a,b}, P. Govoni^{a,b}, M. Malberti^{a,b}, S. Malvezzi^a, A. Massironi^{a,b}, D. Menasce^a, L. Moroni^a, M. Paganoni^{a,b}, D. Pedrini^a, S. Ragazzi^{a,b}, T. Tabarelli de Fatis^{a,b}

INFN Sezione di Napoli ^a, Università di Napoli 'Federico II' ^b, Napoli, Italy, Università della Basilicata ^c, Potenza, Italy, Università G. Marconi ^d, Roma, Italy

S. Buontempo^a, N. Cavallo^{a,c}, A. Di Crescenzo^{a,b}, F. Fabozzi^{a,c}, F. Fienga^a, G. Galati^a, A.O.M. Iorio^{a,b}, W.A. Khan^a, L. Lista^a, S. Meola^{a,d,15}, P. Paolucci^{a,15}, C. Sciacca^{a,b}, E. Voevodina^{a,b}

INFN Sezione di Padova ^a, Università di Padova ^b, Padova, Italy, Università di Trento ^c, Trento, Italy

P. Azzi^a, N. Bacchetta^a, D. Bisello^{a,b}, A. Boletti^{a,b}, A. Bragagnolo, R. Carlin^{a,b}, P. Checchia^a, M. Dall'Osso^{a,b}, P. De Castro Manzano^a, T. Dorigo^a, U. Dosselli^a, F. Gasparini^{a,b}, U. Gasparini^{a,b}, A. Gozzelino^a, S. Lacaprara^a, P. Lujan, M. Margoni^{a,b}, A.T. Meneguzzo^{a,b}, J. Pazzini^{a,b}, P. Ronchese^{a,b}, R. Rossin^{a,b}, F. Simonetto^{a,b}, A. Tiko, E. Torassa^a, M. Zanetti^{a,b}, P. Zotto^{a,b}, G. Zumerle^{a,b}

INFN Sezione di Pavia ^a, Università di Pavia ^b, Pavia, Italy

A. Braghieri^a, A. Magnani^a, P. Montagna^{a,b}, S.P. Ratti^{a,b}, V. Re^a, M. Ressegotti^{a,b}, C. Riccardi^{a,b}, P. Salvini^a, I. Vai^{a,b}, P. Vitulo^{a,b}

INFN Sezione di Perugia ^a, Università di Perugia ^b, Perugia, Italy

L. Alunni Solestizi^{a,b}, M. Biasini^{a,b}, G.M. Bilei^a, C. Cecchi^{a,b}, D. Ciangottini^{a,b}, L. Fanò^{a,b}, P. Lariccia^{a,b}, R. Leonardi^{a,b}, E. Manoni^a, G. Mantovani^{a,b}, V. Mariani^{a,b}, M. Menichelli^a, A. Rossi^{a,b}, A. Santocchia^{a,b}, D. Spiga^a

INFN Sezione di Pisa ^a, Università di Pisa ^b, Scuola Normale Superiore di Pisa ^c, Pisa, Italy

K. Androsov^a, P. Azzurri^a, G. Bagliesi^a, L. Bianchini^a, T. Boccali^a, L. Borrello, R. Castaldi^a, M.A. Ciocci^{a,b}, R. Dell'Orso^a, G. Fedia^a, F. Fiori^{a,c}, L. Giannini^{a,c}, A. Giassi^a, M.T. Grippo^a

F. Ligabue^{a,c}, E. Manca^{a,c}, G. Mandorli^{a,c}, A. Messineo^{a,b}, F. Palla^a, A. Rizzi^{a,b}, P. Spagnolo^a, R. Tenchini^a, G. Tonelli^{a,b}, A. Venturi^a, P.G. Verdini^a

INFN Sezione di Roma ^a, Sapienza Università di Roma ^b, Rome, Italy

L. Barone^{a,b}, F. Cavallari^a, M. Cipriani^{a,b}, N. Daci^a, D. Del Re^{a,b}, E. Di Marco^{a,b}, M. Diemoz^a, S. Gelli^{a,b}, E. Longo^{a,b}, B. Marzocchi^{a,b}, P. Meridiani^a, G. Organtini^{a,b}, F. Pandolfi^a, R. Paramatti^{a,b}, F. Preiato^{a,b}, S. Rahatlou^{a,b}, C. Rovelli^a, F. Santanastasio^{a,b}

INFN Sezione di Torino ^a, Università di Torino ^b, Torino, Italy, Università del Piemonte Orientale ^c, Novara, Italy

N. Amapane^{a,b}, R. Arcidiacono^{a,c}, S. Argiro^{a,b}, M. Arneodo^{a,c}, N. Bartosik^a, R. Bellan^{a,b}, C. Biino^a, N. Cartiglia^a, F. Cenna^{a,b}, S. Cometti, M. Costa^{a,b}, R. Covarelli^{a,b}, N. Demaria^a, B. Kiani^{a,b}, C. Mariotti^a, S. Maselli^a, E. Migliore^{a,b}, V. Monaco^{a,b}, E. Monteil^{a,b}, M. Monteno^a, M.M. Obertino^{a,b}, L. Pacher^{a,b}, N. Pastrone^a, M. Pelliccioni^a, G.L. Pinna Angioni^{a,b}, A. Romero^{a,b}, M. Ruspa^{a,c}, R. Sacchi^{a,b}, K. Shchelina^{a,b}, V. Sola^a, A. Solano^{a,b}, D. Soldi, A. Staiano^a

INFN Sezione di Trieste ^a, Università di Trieste ^b, Trieste, Italy

S. Belforte^a, V. Candelise^{a,b}, M. Casarsa^a, F. Cossutti^a, G. Della Ricca^{a,b}, F. Vazzoler^{a,b}, A. Zanetti^a

Kyungpook National University

D.H. Kim, G.N. Kim, M.S. Kim, J. Lee, S. Lee, S.W. Lee, C.S. Moon, Y.D. Oh, S. Sekmen, D.C. Son, Y.C. Yang

Chonnam National University, Institute for Universe and Elementary Particles, Kwangju, Korea

H. Kim, D.H. Moon, G. Oh

Hanyang University, Seoul, Korea

J. Goh²⁹, T.J. Kim

Korea University, Seoul, Korea

S. Cho, S. Choi, Y. Go, D. Gyun, S. Ha, B. Hong, Y. Jo, K. Lee, K.S. Lee, S. Lee, J. Lim, S.K. Park, Y. Roh

Sejong University, Seoul, Korea

H.S. Kim

Seoul National University, Seoul, Korea

J. Almond, J. Kim, J.S. Kim, H. Lee, K. Lee, K. Nam, S.B. Oh, B.C. Radburn-Smith, S.h. Seo, U.K. Yang, H.D. Yoo, G.B. Yu

University of Seoul, Seoul, Korea

D. Jeon, H. Kim, J.H. Kim, J.S.H. Lee, I.C. Park

Sungkyunkwan University, Suwon, Korea

Y. Choi, C. Hwang, J. Lee, I. Yu

Vilnius University, Vilnius, Lithuania

V. Dudenys, A. Juodagalvis, J. Vaitkus

National Centre for Particle Physics, Universiti Malaya, Kuala Lumpur, Malaysia

I. Ahmed, Z.A. Ibrahim, M.A.B. Md Ali³⁰, F. Mohamad Idris³¹, W.A.T. Wan Abdullah, M.N. Yusli, Z. Zolkapli

Universidad de Sonora (UNISON), Hermosillo, Mexico

A. Castaneda Hernandez, J.A. Murillo Quijada

Centro de Investigacion y de Estudios Avanzados del IPN, Mexico City, Mexico

H. Castilla-Valdez, E. De La Cruz-Burelo, M.C. Duran-Osuna, I. Heredia-De La Cruz³², R. Lopez-Fernandez, J. Mejia Guisao, R.I. Rabadan-Trejo, M. Ramirez-Garcia, G. Ramirez-Sanchez, R Reyes-Almanza, A. Sanchez-Hernandez

Universidad Iberoamericana, Mexico City, Mexico

S. Carrillo Moreno, C. Oropeza Barrera, F. Vazquez Valencia

Benemerita Universidad Autonoma de Puebla, Puebla, Mexico

J. Eysermans, I. Pedraza, H.A. Salazar Ibarguen, C. Uribe Estrada

Universidad Autónoma de San Luis Potosí, San Luis Potosí, Mexico

A. Morelos Pineda

University of Auckland, Auckland, New Zealand

D. Krofcheck

University of Canterbury, Christchurch, New Zealand

S. Bheesette, P.H. Butler

National Centre for Physics, Quaid-I-Azam University, Islamabad, Pakistan

A. Ahmad, M. Ahmad, M.I. Asghar, Q. Hassan, H.R. Hoorani, S. Qazi, M.A. Shah, M. Shoaib, M. Waqas

National Centre for Nuclear Research, Swierk, Poland

H. Bialkowska, M. Bluj, B. Boimska, T. Frueboes, M. Górski, M. Kazana, K. Nawrocki, M. Szleper, P. Traczyk, P. Zalewski

Institute of Experimental Physics, Faculty of Physics, University of Warsaw, Warsaw, Poland

K. Bunkowski, A. Byszuk³³, K. Doroba, A. Kalinowski, M. Konecki, J. Krolikowski, M. Misiura, M. Olszewski, A. Pyskir, M. Walczak

Laboratório de Instrumentação e Física Experimental de Partículas, Lisboa, Portugal

P. Bargassa, C. Beirão Da Cruz E Silva, A. Di Francesco, P. Faccioli, B. Galinhas, M. Gallinaro, J. Hollar, N. Leonardo, L. Lloret Iglesias, M.V. Nemallapudi, J. Seixas, G. Strong, O. Toldaiev, D. Vadrucio, J. Varela

Joint Institute for Nuclear Research, Dubna, Russia

V. Alexakhin, A. Golunov, I. Golutvin, N. Gorbounov, I. Gorbunov, A. Kamenev, V. Karjavin, A. Lanev, A. Malakhov, V. Matveev^{34,35}, P. Moisezenz, V. Palichik, V. Perelygin, M. Savina, S. Shmatov, S. Shulha, N. Skatchkov, V. Smirnov, A. Zarubin

Petersburg Nuclear Physics Institute, Gatchina (St. Petersburg), Russia

V. Golovtsov, Y. Ivanov, V. Kim³⁶, E. Kuznetsova³⁷, P. Levchenko, V. Murzin, V. Oreshkin, I. Smirnov, D. Sosnov, V. Sulimov, L. Uvarov, S. Vavilov, A. Vorobyev

Institute for Nuclear Research, Moscow, Russia

Yu. Andreev, A. Dermenev, S. Gninenko, N. Golubev, A. Karneyeu, M. Kirsanov, N. Krasnikov, A. Pashenkov, D. Tlisov, A. Toropin

Institute for Theoretical and Experimental Physics, Moscow, Russia

V. Epshteyn, V. Gavrillov, N. Lychkovskaya, V. Popov, I. Pozdnyakov, G. Safronov, A. Spiridonov, A. Steppenov, V. Stolin, M. Toms, E. Vlasov, A. Zhokin

Moscow Institute of Physics and Technology, Moscow, Russia

T. Aushev

National Research Nuclear University 'Moscow Engineering Physics Institute' (MEPhI), Moscow, Russia

M. Chadeeva³⁸, P. Parygin, D. Philippov, S. Polikarpov³⁸, E. Popova, V. Rusinov

P.N. Lebedev Physical Institute, Moscow, Russia

V. Andreev, M. Azarkin³⁵, I. Dremine³⁵, M. Kirakosyan³⁵, S.V. Rusakov, A. Terkulov

Skobeltsyn Institute of Nuclear Physics, Lomonosov Moscow State University, Moscow, Russia

A. Baskakov, A. Belyaev, E. Boos, V. Bunichev, M. Dubinin³⁹, L. Dudko, A. Ershov, A. Gribushin, V. Klyukhin, O. Kodolova, I. Lokhtin, I. Miagkov, S. Obraztsov, V. Savrin, A. Snigirev

Novosibirsk State University (NSU), Novosibirsk, Russia

V. Blinov⁴⁰, T. Dimova⁴⁰, L. Kardapoltsev⁴⁰, D. Shtol⁴⁰, Y. Skovpen⁴⁰

State Research Center of Russian Federation, Institute for High Energy Physics of NRC "Kurchatov Institute", Protvino, Russia

I. Azhgirey, I. Bayshev, S. Bitioukov, D. Elumakhov, A. Godizov, V. Kachanov, A. Kalinin, D. Konstantinov, P. Mandrik, V. Petrov, R. Ryutin, S. Slabospitskii, A. Sobol, S. Troshin, N. Tyurin, A. Uzunian, A. Volkov

National Research Tomsk Polytechnic University, Tomsk, Russia

A. Babaev, S. Baidali

University of Belgrade, Faculty of Physics and Vinca Institute of Nuclear Sciences, Belgrade, Serbia

P. Adzic⁴¹, P. Cirkovic, D. Devetak, M. Dordevic, J. Milosevic

Centro de Investigaciones Energéticas Medioambientales y Tecnológicas (CIEMAT), Madrid, Spain

J. Alcaraz Maestre, A. Álvarez Fernández, I. Bachiller, M. Barrio Luna, J.A. Brochero Cifuentes, M. Cerrada, N. Colino, B. De La Cruz, A. Delgado Peris, C. Fernandez Bedoya, J.P. Fernández Ramos, J. Flix, M.C. Fouz, O. Gonzalez Lopez, S. Goy Lopez, J.M. Hernandez, M.I. Josa, D. Moran, A. Pérez-Calero Yzquierdo, J. Puerta Pelayo, I. Redondo, L. Romero, M.S. Soares, A. Triossi

Universidad Autónoma de Madrid, Madrid, Spain

C. Albajar, J.F. de Trocóniz

Universidad de Oviedo, Oviedo, Spain

J. Cuevas, C. Erice, J. Fernandez Menendez, S. Folgueras, I. Gonzalez Caballero, J.R. González Fernández, E. Palencia Cortezon, V. Rodríguez Bouza, S. Sanchez Cruz, P. Vischia, J.M. Vizan Garcia

Instituto de Física de Cantabria (IFCA), CSIC-Universidad de Cantabria, Santander, Spain

I.J. Cabrillo, A. Calderon, B. Chazin Quero, J. Duarte Campderros, M. Fernandez, P.J. Fernández Manteca, A. García Alonso, J. Garcia-Ferrero, G. Gomez, A. Lopez Virto, J. Marco, C. Martinez Rivero, P. Martinez Ruiz del Arbol, F. Matorras, J. Piedra Gomez, C. Prieels, T. Rodrigo, A. Ruiz-Jimeno, L. Scodellaro, N. Trevisani, I. Vila, R. Vilar Cortabitarte

CERN, European Organization for Nuclear Research, Geneva, Switzerland

D. Abbaneo, B. Akgun, E. Auffray, P. Baillon, A.H. Ball, D. Barney, J. Bendavid, M. Bianco,

A. Bocci, C. Botta, E. Brondolin, T. Camporesi, M. Cepeda, G. Cerminara, E. Chapon, Y. Chen, G. Cucciati, D. d'Enterria, A. Dabrowski, V. Daponte, A. David, A. De Roeck, N. Deelen, M. Dobson, T. du Pree, M. Dünser, N. Dupont, A. Elliott-Peisert, P. Everaerts, F. Fallavollita⁴², D. Fasanella, G. Franzoni, J. Fulcher, W. Funk, D. Gigi, A. Gilbert, K. Gill, F. Glege, M. Guilbaud, D. Gulhan, J. Hegeman, V. Innocente, A. Jafari, P. Janot, O. Karacheban¹⁸, J. Kieseler, A. Kornmayer, M. Krammer¹, C. Lange, P. Lecoq, C. Lourenço, L. Malgeri, M. Mannelli, F. Meijers, J.A. Merlin, S. Mersi, E. Meschi, P. Milenovic⁴³, F. Moortgat, M. Mulders, J. Ngadiuba, S. Orfanelli, L. Orsini, F. Pantaleo¹⁵, L. Pape, E. Perez, M. Peruzzi, A. Petrilli, G. Petrucciani, A. Pfeiffer, M. Pierini, F.M. Pitters, D. Rabadý, A. Racz, T. Reis, G. Rolandi⁴⁴, M. Rovere, H. Sakulin, C. Schäfer, C. Schwick, M. Seidel, M. Selvaggi, A. Sharma, P. Silva, P. Sphicas⁴⁵, A. Stakia, J. Steggemann, M. Tosi, D. Treille, A. Tsirou, V. Veckalns⁴⁶, W.D. Zeuner

Paul Scherrer Institut, Villigen, Switzerland

L. Caminada⁴⁷, K. Deiters, W. Erdmann, R. Horisberger, Q. Ingram, H.C. Kaestli, D. Kotlinski, U. Langenegger, T. Rohe, S.A. Wiederkehr

ETH Zurich - Institute for Particle Physics and Astrophysics (IPA), Zurich, Switzerland

M. Backhaus, L. Bäni, P. Berger, N. Chernyavskaya, G. Dissertori, M. Dittmar, M. Donegà, C. Dorfer, C. Grab, C. Heidegger, D. Hits, J. Hoss, T. Klijnsma, W. Lustermann, R.A. Manzoni, M. Marionneau, M.T. Meinhard, F. Micheli, P. Musella, F. Nessi-Tedaldi, J. Pata, F. Pauss, G. Perrin, L. Perrozzi, S. Pigazzini, M. Quittnat, D. Ruini, D.A. Sanz Becerra, M. Schönenberger, L. Shchutska, V.R. Tavolaro, K. Theofilatos, M.L. Vesterbacka Olsson, R. Wallny, D.H. Zhu

Universität Zürich, Zurich, Switzerland

T.K. Aarrestad, C. Amsler⁴⁸, D. Brzhechko, M.F. Canelli, A. De Cosa, R. Del Burgo, S. Donato, C. Galloni, T. Hreus, B. Kilminster, I. Neutelings, D. Pinna, G. Rauco, P. Robmann, D. Salerno, K. Schweiger, C. Seitz, Y. Takahashi, A. Zucchetta

National Central University, Chung-Li, Taiwan

Y.H. Chang, K.y. Cheng, T.H. Doan, Sh. Jain, R. Khurana, C.M. Kuo, W. Lin, A. Pozdnyakov, S.S. Yu

National Taiwan University (NTU), Taipei, Taiwan

P. Chang, Y. Chao, K.F. Chen, P.H. Chen, W.-S. Hou, Arun Kumar, Y.y. Li, Y.F. Liu, R.-S. Lu, E. Paganis, A. Psallidas, A. Steen, J.f. Tsai

Chulalongkorn University, Faculty of Science, Department of Physics, Bangkok, Thailand

B. Asavapibhop, N. Srimanobhas, N. Suwonjandee

Çukurova University, Physics Department, Science and Art Faculty, Adana, Turkey

A. Bat, F. Boran, S. Cerci⁴⁹, S. Damarcekin, Z.S. Demiroglu, F. Dolek, C. Dozen, I. Dumanoglu, S. Girgis, G. Gokbulut, Y. Guler, E. Gurpinar, I. Hos⁵⁰, C. Isik, E.E. Kangal⁵¹, O. Kara, A. Kayis Topaksu, U. Kiminsu, M. Oglakci, G. Onengut, K. Ozdemir⁵², S. Ozturk⁵³, D. Sunar Cerci⁴⁹, B. Tali⁴⁹, U.G. Tok, S. Turkcapar, I.S. Zorbakir, C. Zorbilmez

Middle East Technical University, Physics Department, Ankara, Turkey

B. Isildak⁵⁴, G. Karapinar⁵⁵, M. Yalvac, M. Zeyrek

Bogazici University, Istanbul, Turkey

I.O. Atakisi, E. Gülmez, M. Kaya⁵⁶, O. Kaya⁵⁷, S. Tekten, E.A. Yetkin⁵⁸

Istanbul Technical University, Istanbul, Turkey

M.N. Agaras, S. Atay, A. Cakir, K. Cankocak, Y. Komurcu, S. Sen⁵⁹

Institute for Scintillation Materials of National Academy of Science of Ukraine, Kharkov, Ukraine

B. Grynyov

National Scientific Center, Kharkov Institute of Physics and Technology, Kharkov, Ukraine
L. Levchuk

University of Bristol, Bristol, United Kingdom

F. Ball, L. Beck, J.J. Brooke, D. Burns, E. Clement, D. Cussans, O. Davignon, H. Flacher, J. Goldstein, G.P. Heath, H.F. Heath, L. Kreczko, D.M. Newbold⁶⁰, S. Paramesvaran, B. Penning, T. Sakuma, D. Smith, V.J. Smith, J. Taylor, A. Titterton

Rutherford Appleton Laboratory, Didcot, United Kingdom

K.W. Bell, A. Belyaev⁶¹, C. Brew, R.M. Brown, D. Cieri, D.J.A. Cockerill, J.A. Coughlan, K. Harder, S. Harper, J. Linacre, E. Olaiya, D. Petyt, C.H. Shepherd-Themistocleous, A. Thea, I.R. Tomalin, T. Williams, W.J. Womersley

Imperial College, London, United Kingdom

G. Auzinger, R. Bainbridge, P. Bloch, J. Borg, S. Breeze, O. Buchmuller, A. Bundock, S. Casasso, D. Colling, L. Corpe, P. Dauncey, G. Davies, M. Della Negra, R. Di Maria, Y. Haddad, G. Hall, G. Iles, T. James, M. Komm, C. Laner, L. Lyons, A.-M. Magnan, S. Malik, A. Martelli, J. Nash⁶², A. Nikitenko⁷, V. Palladino, M. Pesaresi, A. Richards, A. Rose, E. Scott, C. Seez, A. Shtipliyski, G. Singh, M. Stoye, T. Strebler, S. Summers, A. Tapper, K. Uchida, T. Virdee¹⁵, N. Wardle, D. Winterbottom, J. Wright, S.C. Zenz

Brunel University, Uxbridge, United Kingdom

J.E. Cole, P.R. Hobson, A. Khan, P. Kyberd, C.K. Mackay, A. Morton, I.D. Reid, L. Teodorescu, S. Zahid

Baylor University, Waco, USA

K. Call, J. Dittmann, K. Hatakeyama, H. Liu, C. Madrid, B. McMaster, N. Pastika, C. Smith

Catholic University of America, Washington DC, USA

R. Bartek, A. Dominguez

The University of Alabama, Tuscaloosa, USA

A. Buccilli, S.I. Cooper, C. Henderson, P. Rumerio, C. West

Boston University, Boston, USA

D. Arcaro, T. Bose, D. Gastler, D. Rankin, C. Richardson, J. Rohlf, L. Sulak, D. Zou

Brown University, Providence, USA

G. Benelli, X. Coubez, D. Cutts, M. Hadley, J. Hakala, U. Heintz, J.M. Hogan⁶³, K.H.M. Kwok, E. Laird, G. Landsberg, J. Lee, Z. Mao, M. Narain, S. Piperov, S. Sagir⁶⁴, R. Syarif, E. Usai, D. Yu

University of California, Davis, Davis, USA

R. Band, C. Brainerd, R. Breedon, D. Burns, M. Calderon De La Barca Sanchez, M. Chertok, J. Conway, R. Conway, P.T. Cox, R. Erbacher, C. Flores, G. Funk, W. Ko, O. Kukral, R. Lander, C. Mclean, M. Mulhearn, D. Pellett, J. Pilot, S. Shalhout, M. Shi, D. Stolp, D. Taylor, K. Tos, M. Tripathi, Z. Wang, F. Zhang

University of California, Los Angeles, USA

M. Bachtis, C. Bravo, R. Cousins, A. Dasgupta, A. Florent, J. Hauser, M. Ignatenko, N. Mccoll, S. Regnard, D. Saltzberg, C. Schnaible, V. Valuev

University of California, Riverside, Riverside, USA

E. Bouvier, K. Burt, R. Clare, J.W. Gary, S.M.A. Ghiasi Shirazi, G. Hanson, G. Karapostoli, E. Kennedy, F. Lacroix, O.R. Long, M. Olmedo Negrete, M.I. Paneva, W. Si, L. Wang, H. Wei, S. Wimpenny, B.R. Yates

University of California, San Diego, La Jolla, USA

J.G. Branson, S. Cittolin, M. Derdzinski, R. Gerosa, D. Gilbert, B. Hashemi, A. Holzner, D. Klein, G. Kole, V. Krutelyov, J. Letts, M. Masciovecchio, D. Olivito, S. Padhi, M. Pieri, M. Sani, V. Sharma, S. Simon, M. Tadel, A. Vartak, S. Wasserbaech⁶⁵, J. Wood, F. Würthwein, A. Yagil, G. Zevi Della Porta

University of California, Santa Barbara - Department of Physics, Santa Barbara, USA

N. Amin, R. Bhandari, J. Bradmiller-Feld, C. Campagnari, M. Citron, A. Dishaw, V. Dutta, M. Franco Sevilla, L. Gouskos, R. Heller, J. Incandela, A. Ovcharova, H. Qu, J. Richman, D. Stuart, I. Suarez, S. Wang, J. Yoo

California Institute of Technology, Pasadena, USA

D. Anderson, A. Bornheim, J.M. Lawhorn, H.B. Newman, T.Q. Nguyen, M. Spiropulu, J.R. Vlimant, R. Wilkinson, S. Xie, Z. Zhang, R.Y. Zhu

Carnegie Mellon University, Pittsburgh, USA

M.B. Andrews, T. Ferguson, T. Mudholkar, M. Paulini, M. Sun, I. Vorobiev, M. Weinberg

University of Colorado Boulder, Boulder, USA

J.P. Cumalat, W.T. Ford, F. Jensen, A. Johnson, M. Krohn, S. Leontsinis, E. MacDonald, T. Mulholland, K. Stenson, K.A. Ulmer, S.R. Wagner

Cornell University, Ithaca, USA

J. Alexander, J. Chaves, Y. Cheng, J. Chu, A. Datta, K. McDermott, N. Mirman, J.R. Patterson, D. Quach, A. Rinkevicius, A. Ryd, L. Skinnari, L. Soffi, S.M. Tan, Z. Tao, J. Thom, J. Tucker, P. Wittich, M. Zientek

Fermi National Accelerator Laboratory, Batavia, USA

S. Abdullin, M. Albrow, M. Alyari, G. Apollinari, A. Apresyan, A. Apyan, S. Banerjee, L.A.T. Bauerdick, A. Beretvas, J. Berryhill, P.C. Bhat, G. Bolla[†], K. Burkett, J.N. Butler, A. Canepa, G.B. Cerati, H.W.K. Cheung, F. Chlebana, M. Cremonesi, J. Duarte, V.D. Elvira, J. Freeman, Z. Gecse, E. Gottschalk, L. Gray, D. Green, S. Grünendahl, O. Gutsche, J. Hanlon, R.M. Harris, S. Hasegawa, J. Hirschauer, Z. Hu, B. Jayatilaka, S. Jindariani, M. Johnson, U. Joshi, B. Klima, M.J. Kortelainen, B. Kreis, S. Lammel, D. Lincoln, R. Lipton, M. Liu, T. Liu, J. Lykken, K. Maeshima, J.M. Marraffino, D. Mason, P. McBride, P. Merkel, S. Mrenna, S. Nahn, V. O'Dell, K. Pedro, C. Pena, O. Prokofyev, G. Rakness, L. Ristori, A. Savoy-Navarro⁶⁶, B. Schneider, E. Sexton-Kennedy, A. Soha, W.J. Spalding, L. Spiegel, S. Stoynev, J. Strait, N. Strobbe, L. Taylor, S. Tkaczyk, N.V. Tran, L. Uplegger, E.W. Vaandering, C. Vernieri, M. Verzocchi, R. Vidal, M. Wang, H.A. Weber, A. Whitbeck

University of Florida, Gainesville, USA

D. Acosta, P. Avery, P. Bortignon, D. Bourilkov, A. Brinkerhoff, L. Cadamuro, A. Carnes, M. Carver, D. Curry, R.D. Field, S.V. Gleyzer, B.M. Joshi, J. Konigsberg, A. Korytov, P. Ma, K. Matchev, H. Mei, G. Mitselmakher, K. Shi, D. Sperka, J. Wang, S. Wang

Florida International University, Miami, USA

Y.R. Joshi, S. Linn

Florida State University, Tallahassee, USA

A. Ackert, T. Adams, A. Askew, S. Hagopian, V. Hagopian, K.F. Johnson, T. Kolberg, G. Martinez, T. Perry, H. Prosper, A. Saha, V. Sharma, R. Yohay

Florida Institute of Technology, Melbourne, USA

M.M. Baarmand, V. Bhopalkar, S. Colafranceschi, M. Hohlmann, D. Noonan, M. Rahmani, T. Roy, F. Yumiceva

University of Illinois at Chicago (UIC), Chicago, USA

M.R. Adams, L. Apanasevich, D. Berry, R.R. Betts, R. Cavanaugh, X. Chen, S. Dittmer, O. Evdokimov, C.E. Gerber, D.A. Hangal, D.J. Hofman, K. Jung, J. Kamin, C. Mills, I.D. Sandoval Gonzalez, M.B. Tonjes, N. Varelas, H. Wang, X. Wang, Z. Wu, J. Zhang

The University of Iowa, Iowa City, USA

M. Alhusseini, B. Bilki⁶⁷, W. Clarida, K. Dilsiz⁶⁸, S. Durgut, R.P. Gandrajula, M. Haytmyradov, V. Khristenko, J.-P. Merlo, A. Mestvirishvili, A. Moeller, J. Nachtman, H. Ogul⁶⁹, Y. Onel, F. Ozok⁷⁰, A. Penzo, C. Snyder, E. Tiras, J. Wetzel

Johns Hopkins University, Baltimore, USA

B. Blumenfeld, A. Cocoros, N. Eminizer, D. Fehling, L. Feng, A.V. Gritsan, W.T. Hung, P. Maksimovic, J. Roskes, U. Sarica, M. Swartz, M. Xiao, C. You

The University of Kansas, Lawrence, USA

A. Al-bataineh, P. Baringer, A. Bean, S. Boren, J. Bowen, A. Bylinkin, J. Castle, S. Khalil, A. Kropivnitskaya, D. Majumder, W. Mcbrayer, M. Murray, C. Rogan, S. Sanders, E. Schmitz, J.D. Tapia Takaki, Q. Wang

Kansas State University, Manhattan, USA

S. Duric, A. Ivanov, K. Kaadze, D. Kim, Y. Maravin, D.R. Mendis, T. Mitchell, A. Modak, A. Mohammadi, L.K. Saini, N. Skhirtladze

Lawrence Livermore National Laboratory, Livermore, USA

F. Rebassoo, D. Wright

University of Maryland, College Park, USA

A. Baden, O. Baron, A. Belloni, S.C. Eno, Y. Feng, C. Ferraioli, N.J. Hadley, S. Jabeen, G.Y. Jeng, R.G. Kellogg, J. Kunkle, A.C. Mignerey, F. Ricci-Tam, Y.H. Shin, A. Skuja, S.C. Tonwar, K. Wong

Massachusetts Institute of Technology, Cambridge, USA

D. Abercrombie, B. Allen, V. Azzolini, A. Baty, G. Bauer, R. Bi, S. Brandt, W. Busza, I.A. Cali, M. D'Alfonso, Z. Demiragli, G. Gomez Ceballos, M. Goncharov, P. Harris, D. Hsu, M. Hu, Y. Iiyama, G.M. Innocenti, M. Klute, D. Kovalskyi, Y.-J. Lee, P.D. Luckey, B. Maier, A.C. Marini, C. McGinn, C. Mironov, S. Narayanan, X. Niu, C. Paus, C. Roland, G. Roland, G.S.F. Stephans, K. Sumorok, K. Tatar, D. Velicanu, J. Wang, T.W. Wang, B. Wyslouch, S. Zhaozhong

University of Minnesota, Minneapolis, USA

A.C. Benvenuti, R.M. Chatterjee, A. Evans, P. Hansen, S. Kalafut, Y. Kubota, Z. Lesko, J. Mans, S. Nourbakhsh, N. Ruckstuhl, R. Rusack, J. Turkewitz, M.A. Wadud

University of Mississippi, Oxford, USA

J.G. Acosta, S. Oliveros

University of Nebraska-Lincoln, Lincoln, USA

E. Avdeeva, K. Bloom, D.R. Claes, C. Fangmeier, F. Golf, R. Gonzalez Suarez, R. Kamalieddin, I. Kravchenko, J. Monroy, J.E. Siado, G.R. Snow, B. Stieger

State University of New York at Buffalo, Buffalo, USA

A. Godshalk, C. Harrington, I. Iashvili, A. Kharchilava, D. Nguyen, A. Parker, S. Rappoccio, B. Roozbahani

Northeastern University, Boston, USA

G. Alverson, E. Barberis, C. Freer, A. Hortiangtham, D.M. Morse, T. Orimoto, R. Teixeira De Lima, T. Wamorkar, B. Wang, A. Wisecarver, D. Wood

Northwestern University, Evanston, USA

S. Bhattacharya, O. Charaf, K.A. Hahn, N. Mucia, N. Odell, M.H. Schmitt, K. Sung, M. Trovato, M. Velasco

University of Notre Dame, Notre Dame, USA

R. Bucci, N. Dev, M. Hildreth, K. Hurtado Anampa, C. Jessop, D.J. Karmgard, N. Kellams, K. Lannon, W. Li, N. Loukas, N. Marinelli, F. Meng, C. Mueller, Y. Musienko³⁴, M. Planer, A. Reinsvold, R. Ruchti, P. Siddireddy, G. Smith, S. Taroni, M. Wayne, A. Wightman, M. Wolf, A. Woodard

The Ohio State University, Columbus, USA

J. Alimena, L. Antonelli, B. Bylsma, L.S. Durkin, S. Flowers, B. Francis, A. Hart, C. Hill, W. Ji, T.Y. Ling, W. Luo, B.L. Winer, H.W. Wulsin

Princeton University, Princeton, USA

S. Cooperstein, P. Elmer, J. Hardenbrook, P. Hebda, S. Higginbotham, A. Kalogeropoulos, D. Lange, M.T. Lucchini, J. Luo, D. Marlow, K. Mei, I. Ojalvo, J. Olsen, C. Palmer, P. Piroué, J. Salfeld-Nebgen, D. Stickland, C. Tully

University of Puerto Rico, Mayaguez, USA

S. Malik, S. Norberg

Purdue University, West Lafayette, USA

A. Barker, V.E. Barnes, S. Das, L. Gutay, M. Jones, A.W. Jung, A. Khatiwada, B. Mahakud, D.H. Miller, N. Neumeister, C.C. Peng, H. Qiu, J.F. Schulte, J. Sun, F. Wang, R. Xiao, W. Xie

Purdue University Northwest, Hammond, USA

T. Cheng, J. Dolen, N. Parashar

Rice University, Houston, USA

Z. Chen, K.M. Ecklund, S. Freed, F.J.M. Geurts, M. Kilpatrick, W. Li, B. Michlin, B.P. Padley, J. Roberts, J. Rorie, W. Shi, Z. Tu, J. Zabel, A. Zhang

University of Rochester, Rochester, USA

A. Bodek, P. de Barbaro, R. Demina, Y.t. Duh, J.L. Dulemba, C. Fallon, T. Ferbel, M. Galanti, A. Garcia-Bellido, J. Han, O. Hindrichs, A. Khukhunaishvili, K.H. Lo, P. Tan, R. Taus, M. Verzetti

Rutgers, The State University of New Jersey, Piscataway, USA

A. Agapitos, J.P. Chou, Y. Gershtein, T.A. Gómez Espinosa, E. Halkiadakis, M. Heindl, E. Hughes, S. Kaplan, R. Kunnawalkam Elayavalli, S. Kyriacou, A. Lath, R. Montalvo, K. Nash, M. Osherson, H. Saka, S. Salur, S. Schnetzer, D. Sheffield, S. Somalwar, R. Stone, S. Thomas, P. Thomassen, M. Walker

University of Tennessee, Knoxville, USA

A.G. Delannoy, J. Heideman, G. Riley, K. Rose, S. Spanier, K. Thapa

Texas A&M University, College Station, USA

O. Bouhali⁷¹, A. Celik, M. Dalchenko, M. De Mattia, A. Delgado, S. Dildick, R. Eusebi, J. Gilmore, T. Huang, T. Kamon⁷², S. Luo, R. Mueller, Y. Pakhotin, R. Patel, A. Perloff, L. Perniè, D. Rathjens, A. Safonov, A. Tatarinov

Texas Tech University, Lubbock, USA

N. Akchurin, J. Damgov, F. De Guio, P.R. Duderø, S. Kunori, K. Lamichhane, S.W. Lee, T. Mengke, S. Muthumuni, T. Peltola, S. Undleeb, I. Volobouev, Z. Wang

Vanderbilt University, Nashville, USA

S. Greene, A. Gurrola, R. Janjam, W. Johns, C. Maguire, A. Melo, H. Ni, K. Padeken, J.D. Ruiz Alvarez, P. Sheldon, S. Tuo, J. Velkovska, M. Verweij, Q. Xu

University of Virginia, Charlottesville, USA

M.W. Arenton, P. Barria, B. Cox, R. Hirosky, M. Joyce, A. Ledovskoy, H. Li, C. Neu, T. Sinthuprasith, Y. Wang, E. Wolfe, F. Xia

Wayne State University, Detroit, USA

R. Harr, P.E. Karchin, N. Poudyal, J. Sturdy, P. Thapa, S. Zaleski

University of Wisconsin - Madison, Madison, WI, USA

M. Brodski, J. Buchanan, C. Caillol, D. Carlsmith, S. Dasu, L. Dodd, B. Gomber, M. Grothe, M. Herndon, A. Hervé, U. Hussain, P. Klabbers, A. Lanaro, A. Levine, K. Long, R. Loveless, T. Ruggles, A. Savin, N. Smith, W.H. Smith, N. Woods

†: Deceased

1: Also at Vienna University of Technology, Vienna, Austria

2: Also at IRFU, CEA, Université Paris-Saclay, Gif-sur-Yvette, France

3: Also at Universidade Estadual de Campinas, Campinas, Brazil

4: Also at Federal University of Rio Grande do Sul, Porto Alegre, Brazil

5: Also at Université Libre de Bruxelles, Bruxelles, Belgium

6: Also at University of Chinese Academy of Sciences, Beijing, China

7: Also at Institute for Theoretical and Experimental Physics, Moscow, Russia

8: Also at Joint Institute for Nuclear Research, Dubna, Russia

9: Also at Suez University, Suez, Egypt

10: Now at British University in Egypt, Cairo, Egypt

11: Also at Zewail City of Science and Technology, Zewail, Egypt

12: Also at Department of Physics, King Abdulaziz University, Jeddah, Saudi Arabia

13: Also at Université de Haute Alsace, Mulhouse, France

14: Also at Skobeltsyn Institute of Nuclear Physics, Lomonosov Moscow State University, Moscow, Russia

15: Also at CERN, European Organization for Nuclear Research, Geneva, Switzerland

16: Also at RWTH Aachen University, III. Physikalisches Institut A, Aachen, Germany

17: Also at University of Hamburg, Hamburg, Germany

18: Also at Brandenburg University of Technology, Cottbus, Germany

19: Also at MTA-ELTE Lendület CMS Particle and Nuclear Physics Group, Eötvös Loránd University, Budapest, Hungary

20: Also at Institute of Nuclear Research ATOMKI, Debrecen, Hungary

21: Also at Institute of Physics, University of Debrecen, Debrecen, Hungary

22: Also at Indian Institute of Technology Bhubaneswar, Bhubaneswar, India

23: Also at Institute of Physics, Bhubaneswar, India

24: Also at Shoolini University, Solan, India

- 25: Also at University of Visva-Bharati, Santiniketan, India
- 26: Also at Isfahan University of Technology, Isfahan, Iran
- 27: Also at Plasma Physics Research Center, Science and Research Branch, Islamic Azad University, Tehran, Iran
- 28: Also at Università degli Studi di Siena, Siena, Italy
- 29: Also at Kyunghee University, Seoul, Korea
- 30: Also at International Islamic University of Malaysia, Kuala Lumpur, Malaysia
- 31: Also at Malaysian Nuclear Agency, MOSTI, Kajang, Malaysia
- 32: Also at Consejo Nacional de Ciencia y Tecnología, Mexico city, Mexico
- 33: Also at Warsaw University of Technology, Institute of Electronic Systems, Warsaw, Poland
- 34: Also at Institute for Nuclear Research, Moscow, Russia
- 35: Now at National Research Nuclear University 'Moscow Engineering Physics Institute' (MEPhI), Moscow, Russia
- 36: Also at St. Petersburg State Polytechnical University, St. Petersburg, Russia
- 37: Also at University of Florida, Gainesville, USA
- 38: Also at P.N. Lebedev Physical Institute, Moscow, Russia
- 39: Also at California Institute of Technology, Pasadena, USA
- 40: Also at Budker Institute of Nuclear Physics, Novosibirsk, Russia
- 41: Also at Faculty of Physics, University of Belgrade, Belgrade, Serbia
- 42: Also at INFN Sezione di Pavia ^a, Università di Pavia ^b, Pavia, Italy
- 43: Also at University of Belgrade, Faculty of Physics and Vinca Institute of Nuclear Sciences, Belgrade, Serbia
- 44: Also at Scuola Normale e Sezione dell'INFN, Pisa, Italy
- 45: Also at National and Kapodistrian University of Athens, Athens, Greece
- 46: Also at Riga Technical University, Riga, Latvia
- 47: Also at Universität Zürich, Zurich, Switzerland
- 48: Also at Stefan Meyer Institute for Subatomic Physics (SMI), Vienna, Austria
- 49: Also at Adiyaman University, Adiyaman, Turkey
- 50: Also at Istanbul Aydin University, Istanbul, Turkey
- 51: Also at Mersin University, Mersin, Turkey
- 52: Also at Piri Reis University, Istanbul, Turkey
- 53: Also at Gaziosmanpasa University, Tokat, Turkey
- 54: Also at Ozyegin University, Istanbul, Turkey
- 55: Also at Izmir Institute of Technology, Izmir, Turkey
- 56: Also at Marmara University, Istanbul, Turkey
- 57: Also at Kafkas University, Kars, Turkey
- 58: Also at Istanbul Bilgi University, Istanbul, Turkey
- 59: Also at Hacettepe University, Ankara, Turkey
- 60: Also at Rutherford Appleton Laboratory, Didcot, United Kingdom
- 61: Also at School of Physics and Astronomy, University of Southampton, Southampton, United Kingdom
- 62: Also at Monash University, Faculty of Science, Clayton, Australia
- 63: Also at Bethel University, St. Paul, USA
- 64: Also at Karamanoğlu Mehmetbey University, Karaman, Turkey
- 65: Also at Utah Valley University, Orem, USA
- 66: Also at Purdue University, West Lafayette, USA
- 67: Also at Beykent University, Istanbul, Turkey
- 68: Also at Bingol University, Bingol, Turkey
- 69: Also at Sinop University, Sinop, Turkey

70: Also at Mimar Sinan University, Istanbul, Istanbul, Turkey

71: Also at Texas A&M University at Qatar, Doha, Qatar

72: Also at Kyungpook National University, Daegu, Korea